Atmos. Meas. Tech. Discuss., doi:10.5194/amt-2016-337, 2016
Manuscript under review for journal Atmos. Meas. Tech.
Published: 9 November 2016

Atmospheric Measurement Techniques Discussions

Evaluation of the new capture vaporizer for Aerosol Mass Spectrometers (AMS) through laboratory studies of inorganic species

Weiwei Hu[1,2], Pedro Campuzano-Jost[1,2], Douglas A. Day[1,2], Philip Croteau[3], Manjula R. Canagaratna[3], John T. Jayne[3], Douglas R. Worsnop[3], Jose L. Jimenez[1,2]

1 Cooperative Institute for Research in the Environmental Sciences (CIRES), University of Colorado at Boulder, 216 UCB, Boulder, CO 80309, USA

2 Department of Chemistry & Biochemistry, University of Colorado at Boulder, 216 UCB, Boulder, CO 80309, USA

3 Aerodyne Research, Inc., Billerica, Massachusetts, USA

Correspondence to: J. L. Jimenez (jose.jimenez@colorado.edu)

Abstract

Aerosol mass spectrometers (AMS) and Aerosol Chemical Speciation Monitors (ACSM) commercialized by Aerodyne Research Inc. are used widely to measure the mass concentrations and size distributions of non-refractory species in submicron-particles. With the "standard" vaporizer (SV) that is installed in all commercial instruments to date, the quantification of ambient aerosol mass concentration requires the use of a collection efficiency (CE) for correcting the loss of particles due to bounce on the SV. However, CE depends on aerosol phase, and thus can vary with location, airmass, and season of sampling. Although a composition-dependent parameterization of CE in the SV for ambient data has been successful, CE still contributes most of the estimated uncertainty to reported concentrations, and is also an important uncertainty in laboratory studies. To address this limitation, a new "capture" vaporizer (CV) has been designed to reduce or eliminate particle bounce and thus the need for a CE correction.

To test the performance of the CV, two high-resolution AMS instruments, one with a SV and one with a CV were operated side by side in the laboratory. Four standard species NH_4NO_3, $NaNO_3$, $(NH_4)_2SO_4$ and NH_4Cl, which typically constitute the majority of the mass of ambient submicron inorganic species, are studied. The effect of vaporizer temperature (T_v~200-800℃) on the detected fragments, CE and size distributions are investigated. A T_v of 500-550℃ for the CV is recommended based on the observed performance. In the CV, CE was identical (around unity) for more volatile species and comparable or higher compared to the SV for less volatile species, demonstrating a substantial improvement in CE of inorganic species in the CV. The detected fragments of NO_3 and SO_4 species observed with the CV are different than those observed with the SV, suggesting additional thermal decomposition arising from the increased residence time and hot surface collisions. Longer particle detection times lead to broadened particle size distribution measurements made with the AMS. The degradation of CV size distributions due to this broadening is significant for laboratory studies using monodisperse particles, but minor for field studies since ambient distributions are typically quite broad. A method for estimating whether pure species will be detected in AMS sizing mode is proposed. Production of $CO_2(g)$ from sampled nitrate on the vaporizer surface, which has been reported for the SV, is negligible for the CV for NH_4NO_3 and comparable to the SV for $NaNO_3$. Adjusting the alignment of aerodynamic lens to focus particles on the edge of the CV results in higher resolution size distributions, which can be useful in some laboratory experiments. We observe an extremely consistent detection of ammonium from different inorganic ammonium salts, independent of the vaporizer types and/or the T_v. This contradicts a recent suggestion by Murphy (2016) that inorganic species evaporate as intact salts in the AMS.

Atmos. Meas. Tech. Discuss., doi:10.5194/amt-2016-337, 2016
Manuscript under review for journal Atmos. Meas. Tech.
Published: 9 November 2016

Atmospheric Measurement Techniques Discussions

1 INTRODUCTION

Submicron aerosols have major effects on climate and human health (Hallquist et al., 2009; Heal et al., 2012; IPCC, 2013; Fuzzi et al., 2015). In recent decades, various new instruments have been developed to measure different properties of fine aerosols (Turpin et al., 2000; Farmer and Jimenez, 2010). Among them, aerosol mass spectrometers (AMS, produced by Aerodyne Research Inc., Billerica, MA, USA) have emerged as one of the most commonly used on-line aerosol composition instruments due to their fast-response (~seconds to minutes) and ability to quantify the bulk chemical composition and size distribution of sub-micron non-refractory aerosols, i.e. organic aerosol, sulfate, ammonium, nitrate and chloride (Jayne et al., 2000; Allan et al., 2003a; Allan et al., 2003b; Canagaratna et al., 2007; Jimenez et al., 2009 and references therein).

Comparisons between AMS and other co-located aerosol instruments in various field studies (Drewnick et al., 2003; Allan et al., 2004a; Drewnick et al., 2004b; Takegawa et al., 2009; Docherty et al., 2011; Middlebrook et al., 2012) or laboratory studies (Bahreini et al., 2005; Matthew et al., 2008; Docherty et al., 2012) have shown that, despite the typically strong correlation between AMS and other aerosol instrument measurements, a correction factor needs to be used for mass quantification in the AMS. This factor is known to be due predominately to the AMS collection efficiency (CE), which is the ratio between concentration of particles detected in AMS versus concentration of particles introduced to AMS inlet (Huffman et al., 2005; Matthew et al., 2008). CE < 1 in the AMS can be due to particle loss within the (1) aerodynamic lens (E_L), depending on particle size, lens design and pressure (Jayne et al., 2000; Liu et al., 2007; Bahreini et al., 2008); (2) particle time-of-flight (PToF) chamber (E_S) caused by non-spherical particles that result in broader particle beams with some particles not reaching the

Atmos. Meas. Tech. Discuss., doi:10.5194/amt-2016-337, 2016
Manuscript under review for journal Atmos. Meas. Tech.
Published: 9 November 2016

vaporizer (Huffman et al., 2005; Salcedo et al., 2007), or (3) particle bounce on the vaporizer (E_B). The final CE is the product of these three factors (CE = $E_L \times E_S \times E_B$) (Huffman et al., 2005). Multiple laboratory and field measurements have shown that E_L and E_S are typically near unity for submicron particles, whereas E_B is the dominant term (Matthew et al., 2008; Middlebrook et al., 2012). All AMS commercial instruments to date have used a "standard vaporizer" (SV), shaped as an inverted cone of porous tungsten, and kept at vaporizer temperature (T_v) of ~ 550-600 ℃ for ambient measurements (and most laboratory measurements).

Various factors including RH in the sampling line, aerosol water content, aerosol acidity/neutralization of sulfate content and ammonium nitrate fraction in total aerosol, can influence CE, and thus aerosol quantification in the AMS (Quinn et al., 2006; Middlebrook et al., 2012). CE in the SV ranges 0.2-0.4 for pure ammonium sulfate (Drewnick et al., 2004a; Weimer et al., 2006; Takegawa et al., 2009) and ~1 for pure ammonium nitrate (Jayne et al., 2000; Middlebrook et al., 2012). A parameterization of CE for ambient particles based on composition has been used successfully in many environments (Middlebrook et al., 2012), but the remaining uncertainties on CE are thought to dominate the uncertainty of AMS concentration measurements (Bahreini et al., 2009)

Efforts aiming to minimize the uncertainty of aerosol mass spectrometers have been conducted recently. Using the differential mobility analyzer (DMA)-impactor technique, Kang et al. (2015) tested different metal materials, vaporizer surfaces and shapes for particle bouncing and found copper, meshed/porous surface, as well as reversed T shape best at reducing the particle bounce fraction. Each version can reduce the bounce fraction around 10-50% compared to the basic setup, indicating CE can be improved through vaporizer design. A custom instrument similar to the AMS has a different design of particle trap/vaporizer to increase CE (Takegawa et

Atmos. Meas. Tech. Discuss., doi:10.5194/amt-2016-337, 2016
Manuscript under review for journal Atmos. Meas. Tech.
Published: 9 November 2016

al., 2012; Ozawa et al., 2016). A regression slope for 0.7 of sulfate in a field study was observed between this and other instruments.

A "capture vaporizer" (CV) has been recently developed by Aerodyne (Jayne and Worsnop, 2016), aiming to achieve CE = 1 for ambient particles in the AMS, hence decrease the quantification uncertainty (Xu et al., 2016). We have performed laboratory studies to evaluate the performance and detection characteristics of the CV for key inorganic species, i.e., NH_4NO_3, $NaNO_3$, $(NH_4)_2SO_4$ and NH_4Cl. We compare fragmentation patterns, CE and particle size distributions a function of T_v (= 200-800℃) in both SV and CV. This is the first time that the performance of laboratory-generated inorganic aerosol in AMS with the SV and CV over a wide range of T_v (200-800℃) has been reported. Recommendations for optimal T_v and fragmentation table modifications for the CV are given. The effect of particle beam position on the vaporizers on the fragmentation and quantification of NH_4NO_3 is also investigated. Finally, we investigate the production of CO_2 in the vaporizer while sampling nitrate in the CV.

2 EXPERIMENTAL SETUP AND INSTRUMENTATION

2.1 Brief description of the capture vaporizer

The detailed design of CV has been presented in Xu et al. (2016), thus only a brief description is provided here. Both the SV and CV are based on cartridge heaters, which are resistively heated by passing power through a ~0.1 mm diameter coiled tungsten wire positioned inside of the tube (Jayne et al., 2000; Canagaratna et al., 2007; Xu et al., 2016). The CV tube length is about double that of the SV (Fig. S1). The particle impact surface of the SV is an inverted cone, whereas the CV is designed to have a cage inside the vaporizer with a narrow

Atmos. Meas. Tech. Discuss., doi:10.5194/amt-2016-337, 2016
Manuscript under review for journal Atmos. Meas. Tech.
Published: 9 November 2016

entrance (Fig. 1a), designed to minimize particle bouncing loss. The SV is constructed from 80% dense porous tungsten, while the CV is solid molybdenum.

2.2 Laboratory measurement setup

Laboratory experiments in this study were setup as shown in Fig. 1b. Pure inorganic salt particles were generated with a Collison atomizer (model: 3076; TSI, US) from their dilute water solutions. Atomized particles were dried with a Nafion dryer (MD-110-24S-4, Perma Pure LCC, US, RH < 30%), and then were size-selected by a differential mobility analyzer (DMA, model: 3080, TSI, US). To remove multiply-charged particles (required for accurate quantification), impactors with different sizes (i.e. 0.0701cm, 0.0580 cm or 0.0485 cm) were used upstream of the DMA. Finally, the monodisperse particles were measured by two nominally identical high-resolution time-of-flight AMS (HR-ToF-AMS) equipped with SV and CV, respectively. Particle number concentration was determined with a condensation particle counter (CPC, model: 3760 or 3010, TSI, US) sampling in parallel to the AMSs. The mass concentrations can be calculated from the CPC and size data.

The volume flow rate into the AMS was ~0.1 L min^{-1}. A bypass flow (0.2-0.3 L min^{-1}) near the inlet of each AMS was added to reduce time in the tubing and thus particle losses. Sampling tubes were usually copper or stainless steel of ¼ inch outer diameter. All of the standard inorganic chemical compounds used in this study were analytical grade (purity > 99.9%). Water used was either NERL reagent grade water from Thermo Scientific Inc. (USA) or milli-Q water purified by a Milli-Q Integral Water Purification System (EMD Millipore Corporation, Germany).

2.3 AMS measurements

Atmos. Meas. Tech. Discuss., doi:10.5194/amt-2016-337, 2016
Manuscript under review for journal Atmos. Meas. Tech.
Published: 9 November 2016

In this study, most of the comparison experiments were conducted using HR-ToF-AMSs (DeCarlo et al., 2006). The one exception was the lens alignment experiment for the SV which was carried out in a quadrupole AMS (Q-AMS, Jayne et al., 2000). ToF-AMS data was analyzed with the standard software packages (Squirrel version ≥ 1.52M and PIKA version ≥ 1.12). The Q-AMS data was analyzed with the Q-AMS analysis toolkit (version 1.43). All the ToF MS mode data used in this study was high resolution (HR) data and PToF data was unit mass resolution (UMR) data.

Before each set of experiments, a lens alignment was performed on each AMS. Mass concentrations of detected aerosols were obtained from "MS-mode" signal which is the difference signal between chopper blocking and not blocking the particle beam: "beam open" (6 or 5 s) minus "beam closed" (4 or 5 s) (Jimenez et al., 2003). The ionization and detection efficiency (IE) of nitrate and the relative ionization efficiency (RIE) of ammonium were calibrated with dry monodisperse 400 nm ammonium nitrate (NH_4NO_3) particles every few days during the laboratory studies (Canagaratna et al., 2007). Both BFSP (brute-force single particle mode; DeCarlo et al., 2006) and CPC methods (described above) were applied to the SV AMS, while only the latter method was applied to the CV AMS.

It is not possible to apply the BFSP method to the CV AMS due to the longer residence time of evaporated molecules in the CV resulting in broadening of single-particle pulse so that their signal cannot be sufficiently discriminated from the noise, at least for particle sizes with 90% transmission into the AMS (400 nm NH_4NO_3). The escape time of NH_4NO_3 vapors from the CV is larger than 200 μs (see section 3.1.4), which is much longer than the measured duration of single particle event of NH_4NO_3 in the SV of ~25-40 μs (Drewnick et al., 2015). For other

Atmos. Meas. Tech. Discuss., doi:10.5194/amt-2016-337, 2016
Manuscript under review for journal Atmos. Meas. Tech.
Published: 9 November 2016

species such as $(NH_4)_2SO_4$ an additional cause of broadening is due to additional particle collisions inside the CV, after an initial bounce event.

Most of IE calibrations in AMS were done simultaneously for both AMSs using the same stream of calibrant particles. Sulfate RIE (RIE_{SO4}) was calibrated with pure ammonium sulfate ($(NH_4)_2SO_4$) by measuring the relative response of ammonium in both NH_4NO_3 and $(NH_4)_2SO_4$. T_v in the range of 200-800℃ were used in both AMSs to investigate the influences of this parameter. Chloride RIE applied in this study is 1.3.

2.4 Determination of vaporizer temperature (T_v)

T_v is a function of the electrical power (voltage×current) supplied to the vaporizer, and is controlled by the "electronics box" (EBOX) in the AMS. T_v can be quantified in two ways. One method is through a thermocouple attached to the vaporizer body. The relationship between the thermocouple reading vs applied vaporizer power for the SV and CV are shown in Fig. 2a. The curve for the SV was obtained based on a combination of thermocouple-power readings from several different AMSs (Williams, 2010). The thermocouple reading vs vaporizer power for the CV in our AMS was similar to the SV when vaporizer power was below 2 watts. However, it was lower when vaporizer power was between 2 and 10 watts. In both vaporizers, neither thermocouple measured the actually surface T_v that the particles actually encounter but reasonably close, since the thermocouples were mounted outside out the vaporizer body (Fig. 1a and Fig. S1). The thermocouple reading method usually works well for newly installed vaporizers. However, with vaporizer aging, the thermocouple often becomes detached and hence reports a lower T_v reading than the true values (Williams, 2010). The actually input vaporizer power is likely to be more reliable than the thermocouple reading in most of the conditions.

Atmos. Meas. Tech. Discuss., doi:10.5194/amt-2016-337, 2016
Manuscript under review for journal Atmos. Meas. Tech.
Published: 9 November 2016

Atmospheric Measurement Techniques Discussions

Thus, an alternative method to determine T_v without the thermocouple can be useful. Williams (2010) reported that the measured size distribution width (quantified as the full width at half maximum, FWHM) of the NO_3 signal from monodisperse $NaNO_3$ particles starts to broaden at T_v below 600℃ (±50℃) for SV. This broadening was repeatable in different AMS systems and was proposed as a technique to verify T_v settings. This method is expected to allow identification of problems with the thermocouple measurement, since it directly reflects the chemical evaporation properties of a standard compound. In this study, size distributions of monodisperse 300 nm $NaNO_3$ particles were measured at different T_v (300-800℃) multiple times (2014-2016). A summary of those results for $NaNO_3$ size distributions of FWHM as a function of vaporizer power is displayed in Fig. 2b. The FWHM of $NaNO_3$ for the SV in our AMS was consistent with results from Williams (2010). In the 2014 measurements, the broadening threshold temperature of the SV corresponded to a higher nominal vaporizer power than the others. It was found that the AMS temperature readout ("AMS EBOX") at that time was delivering less power to vaporizer than the readout indicated. Thus, the T_v was corrected by matching the 2014 curve to the others as shown in Fig. 2b. The FWHM as a function of T_v in the CV was consistent among experiments conducted at different instrument conditions during different years, and started to broaden at CV powers of around ~3.6-4 W, which is similar to SV. The reported T_v in this manuscript are based on the relationship of T_v vs vaporizer power shown in Fig. 2a. Finally, 3.8 W and 4.2 W corresponded to $T_v \approx 600$℃ in the SV and CV, respectively.

2.5 SMPS measurements

SMPS particle sizing was verified with monodisperse polystyrene latex spheres (PSLs) (Duke Scientific, Palo Alto, CA, US) with diameters of 250-400 nm. The SMPS sheath and sample flow rates were calibrated before each sets of experiments. Mass concentrations were

Atmos. Meas. Tech. Discuss., doi:10.5194/amt-2016-337, 2016
Manuscript under review for journal Atmos. Meas. Tech.
Published: 9 November 2016

calculated by multiplying reported volume concentrations with their corresponding densities. The densities used for NH_4NO_3, $NaNO_3$, $(NH_4)_2SO_4$ and NH_4Cl in this study are 1.72, 2.26, 1.78 and 1.52 g cm^{-3}, respectively (Haynes, 2015). A "Jayne shape factor" of 0.8 was applied to NH_4NO_3. This Jayne shape factor was experimentally determined by comparing the mobility and vacuum aerodynamic diameters (d_{va}) measured for NH_4NO_3 (Jayne et al., 2000; DeCarlo et al., 2004), and used to correct for the fact that the effective density of pure NH_4NO_3 particles is less than the bulk density.

3 RESULTS AND DISCUSSION

3.1 Thermal decomposition & fragmentation of standard species

3.1.1 Nitrate and sulfate fragmentation patterns.

The fragment ion comparisons of NH_4NO_3 and $(NH_4)_2SO_4$ particles in an argon flow (to remove interfering ions from air) between the SV and CV for T_v ~500-550℃ are shown in Table 1. The major ions of nitrate in NH_4NO_3 are NO^+ and NO_2^+, comprising of ~98% of the signal in the SV and 99% in the CV (Table 1, Jayne et al., 2000; Allan et al., 2004b; Hogrefe et al., 2004). NO_2^+ and NO^+ showed strong linear correlations across a wide range of NH_4NO_3 mass concentrations, as expected (Fig. 3a). The ratio of NO_2^+/NO^+ of NH_4NO_3 in SV was ~0.35, within the range of NO_2^+/NO^+ ratios reported in other studies (0.29-0.75) (Hogrefe et al., 2004; Bae et al., 2007; Farmer and Jimenez, 2010; Fry et al., 2013). In contrast, in the CV it was only 0.04-0.07, an order of magnitude lower. To qualitatively interpret this difference, a possible mechanism of NO_2^+ and NO^+ production in the AMS system is discussed.

Nitrate from NH_4NO_3 particles can produce gas-phase $HNO_3(g)$, $NO_2(g)$ and $NO(g)$ species (Drewnick et al., 2015), as:

Atmos. Meas. Tech. Discuss., doi:10.5194/amt-2016-337, 2016
Manuscript under review for journal Atmos. Meas. Tech.
Published: 9 November 2016

$$NH_4NO_3(s) \rightarrow a\times NH_3(g) + b\times HNO_3(g) + c\times NO_2(g) + d\times NO(g) + \text{others} \quad [1]$$

The electron ionization (EI) fragmentation products of $HNO_3(g)$ and $NO_2(g)$ at 70 eV are mostly NO^+ and NO_2^+, with NO_2^+/NO^+ ratios of ~1.17-2 and 0.3-0.5, respectively (Friedel et al., 1959; Linstrom and Mallard, 2016). $NO(g)$ produces almost only NO^+, and no NO_2^+ (Linstrom and Mallard, 2016). In the AMS (with SV) the fragments observed are often smaller, due to thermal decomposition and fragmentation of hotter ions, given the higher temperatures of the neutrals compared to NIST (Canagaratna et al., 2015). Taking the NIST ratios as upper limits, the NO_2^+/NO^+ ratio in the SV (0.29-0.75) might result from a combination of EI ionization from $HNO_3(g)$, $NO_2(g)$ and $NO(g)$. Pieber et al. (2016) speculated that the $NO_2(g)$ is an important thermal decomposition product for NH_4NO_3 in SV. The NO_2^+/NO^+ ratio in the CV (0.04-0.07) was much lower than NIST ratios from $NO_2(g)$ and $HNO_3(g)$ (0.3-2), suggesting the ionization of $NO(g)$ is likely the major pathway for CV. The dominance of $NO(g)$ in the CV may be due to the longer residence time and increased collisions of vapors in the CV, leading to enhanced thermal decomposition. Indeed, $NO(g)$ is also the favored thermodynamic product for T_v of ~500-650℃ (Wang et al., 2015).

A shift to smaller molecular weight ion fragments for the CV was observed for $(NH_4)_2SO_4$ as well (Fig. 3b). The thermal decomposition products of $(NH_4)_2SO_4$ are shown below:

$$(NH_4)_2SO_4(s) \rightarrow a\times NH_3(g) + b\times H_2SO_4(g) + c\times SO_3(g) + d\times SO_2(g) + e\times H_2O + \text{others} \quad [2]$$

The major ions from sulfate aerosols in the AMS are SO^+, SO_2^+, SO_3^+, HSO_3^+ and $H_2SO_4^+$ (Allan et al., 2004b; Hogrefe et al., 2004). Ratios of SO_3^+, HSO_3^+ and $H_2SO_4^+$ to SO^+ signal in the CV (< 0.05) were consistently lower than for SV (0.11-0.38), while the SO_2^+/SO^+ showed the opposite trend (1.7-1.8 in CV vs 1.0-1.5 in SV). This shift indicates that greater thermal

Atmos. Meas. Tech. Discuss., doi:10.5194/amt-2016-337, 2016
Manuscript under review for journal Atmos. Meas. Tech.
Published: 9 November 2016

decomposition and/or ion fragmentation occurs in the CV. The ratios of SO_3^+ , HSO_3^+ and $H_2SO_4^+$ vs SO^+ from $H_2SO_4(g)$ in standard EI are 2.0, 1.4 and 0.9, respectively (Linstrom and Mallard, 2016). The much lower ratios from $(NH_4)_2SO_4$ (0.11-0.38) in the SV are indicative of substantial thermal decomposition occurring with the SV, which is even larger in the CV,

Standard 70 eV EI of $SO_2(g)$ and $H_2SO_4(g)$ yield SO_2^+/SO^+ of ~2 and ~1, respectively (Linstrom and Mallard, 2016). Therefore, a possible explanation for the higher SO_2^+/SO^+ in the CV is that enhanced thermal decomposition in the CV produces more $SO_2(g)$ than in the SV.

Although the exact ion ratios from each standard species are sensitive to the history and status (e.g., tuning or T_v) of a specific AMS, and can also vary among different AMSs, observation of larger fragments from NO_3 and SO_4 in the SV (vs CV) just described were consistent across all experiments over several years.

3.1.2 *Recommended adjustments to the fragmentation table for H_2O^+ and S^+ in the CV.*

Since the detection of nitrate and sulfate is different in the SV vs CV, accurate quantification for the CV requires the use of an RIE_{SO4} determined with the CV. RIE_{SO4} ~1.2 was found in SV in this study, the same as the default value in the AMS analysis software. RIE_{SO4} in the CV in this study was ~1.7-2.4, significantly larger than in the SV.

The fragmentation tables used in the AMS software also need an adjustment for accurate mass quantification, as the contribution of ammonium sulfate to H_2O^+ and S^+ are different for the CV. The recommended fragmentation table for the CV is shown in Table 2 based on the fragmentation pattern obtained in Table 1. These modifications need to be made for both the UMR and HR fragmentation tables. We note that the determination of sulfate and nitrate in

Atmos. Meas. Tech. Discuss., doi:10.5194/amt-2016-337, 2016
Manuscript under review for journal Atmos. Meas. Tech.
Published: 9 November 2016

mixed inorganic/organic aerosols (e.g., ambient air) includes subtraction of organic interference at several inorganic ions (Allan et al., 2004b). As the fragmentation of organics is also different in the CV, it is expected that some fragmentation table entries that affect sulfate quantification (in particular frag_SO_3[48] and [64]) will need revision for accurate quantification of mixed aerosols from UMR data. We note that those the corrections can vary depending on the type of organics sampled, especially in laboratory and source studies, and thus individual users should always examine those corrections for specific experiments, and modify them if needed.

3.1.3 Effect of T_v

T_v can substantially impact evaporation and thermal decomposition, and hence the fragmentation patterns as well as quantification in the AMS (Canagaratna et al., 2015; Docherty et al., 2015). The T_v-dependent fragmentation patterns can help understand the detection process for both vaporizers, and also help determine the optimum T_v for CV. In this study, fragmentation patterns of four inorganic standards (NH_4NO_3, $NaNO_3$, $(NH_4)_2SO_4$, and NH_4Cl) over the whole usable range of T_v (200-800℃) in both SV and CV are explored (Fig. 4).

NH_4NO_3

In SV, NO_2^+/NO^+ from NH_4NO_3 decreased ~40% as T_v increased from 200℃ to 750℃ (Fig. 4a). A possible explanation for this decreasing trend is that higher T_v increases the fraction of the nitrate thermally decomposing into smaller molecules. For the CV, NO_2^+/NO^+ showed less dependence on temperature and was an order of magnitude lower (0.015-0.04) as discussed above. NO_2^+/NO^+ in the CV at T_v = 200℃ (0.04) was much lower than in SV at T_v = 750℃ (0.5), suggesting the thermal decomposition was stronger in the CV even at low T_v due to the increased vapor collisions and residence time.

$NaNO_3$

Atmos. Meas. Tech. Discuss., doi:10.5194/amt-2016-337, 2016
Manuscript under review for journal Atmos. Meas. Tech.
Published: 9 November 2016

Atmospheric Measurement Techniques Discussions

$NaNO_3$ is less volatile than NH_4NO_3 with melting and boiling points of 306 and 380℃ respectively, substantially are higher than for NH_4NO_3 (melting point of 169℃ and boiling point of ~210℃; Haynes, 2015). In SV, NO_2^+/NO^+ ratio for $NaNO_3$ ranged from 0.1 at 200℃ and 0.005 at 550℃, which is 10-100 times lower than typical values from NH_4NO_3 (0.29-0.75) (Fig. 4b). Much lower NO_2^+/NO^+ from $NaNO_3$ compared to NH_4NO_3 at T_v = 600℃ have also been reported in prior studies with SV in AMS (Bruns et al., 2010). A greater thermal decomposition due to a longer residence time of the particles on the vaporizer surface (resulting from slower evaporation) for $NaNO_3$ than NH_4NO_3, as well as different thermal decomposition pathways (as $NaNO_3$ cannot produce $HNO_3(g)$) are two possible explanations. In the CV, much lower NO_2^+/NO^+ ratios for $NaNO_3$ (0001-0.006) were observed compared to those from the SV (0.01-0.03) and also show less dependence on T_v consistent with the results for NH_4NO_3.

$(NH_4)_2SO_4$

Some T_v-dependent changes of SO_x^+/SO^+ ratios were observed for both vaporizers (Fig. 4c). As the T_v increased, the relative abundance of the heavier ions (HSO_3^+ and SO_3^+) decreased and SO_2^+/SO^+ increased, consistent with increasing thermal decomposition. In contrast to the continuous variation of SO_x^+/SO^+ ratios in the SV over the entire T_v range, the CV only showed a change of SO_x^+/SO^+ below T_v = 300℃ and then leveled off. This indicates that the thermal decomposition of sulfate (within several-second timescale of MS mode) is complete in the CV at T_v > 300℃.

NH_4Cl

The thermal decomposition of NH_4Cl particles is expected to occur through the reaction (Zhu et al., 2007): $NH_4Cl(s) \rightarrow NH_3(g) + HCl(g)$. The main fragments from chloride in the AMS are HCl^+ and Cl^+ (Allan et al., 2004b). In this study, Cl^+/ HCl^+ vs T_v from both vaporizers are

Atmos. Meas. Tech. Discuss., doi:10.5194/amt-2016-337, 2016
Manuscript under review for journal Atmos. Meas. Tech.
Published: 9 November 2016

within a narrow range (0.17-0.27), which is similar to the 70 eV EI fragmentation pattern of HCl(*g*) in the NIST database (Cl+/ HCl+ =~0.17; Linstrom and Mallard, 2016) and also consistent with the Cl^+/HCl^+ ratio observed in other ambient datasets (0.175-0.24) (Hu et al., 2016). Compared to much larger changes for NO_3 and SO_4 fragment ion ratios, the differences in HCl^+/Cl^+ ratio between the vaporizers and temperatures are relatively small. This suggests Cl^+ and HCl^+ that the thermal decomposition and ionization fragmentation of NH_4Cl particle is similar for both vaporizers across different temperatures, and likely mainly from produced from direct ionization of HCl(*g*). We note that unlike NO_3 or SO_4, HCl(*g*) does not have a thermal decomposition pathway.

The small variations of Cl^+/HCl^+ vs T_v may have been due to the changing background of Cl^+ and HCl^+ due to the stickiness of HCl(*g*) on the vaporizer surface and ionization chamber walls. Drewnick et al. (2015) reported that Cl^+ had a slowly evolving background signal (8 to > 30 min at T_v ~600-720℃). We evaluated this effect by examining Cl^+/HCl^+ at the same T_v (~600℃) after increasing T_v from ~600℃ to 850℃, and then returning to 600℃. We found that Cl^+/HCl^+ decreased 25% in the SV and 5% in the CV compared to the values before T_v changing (Fig. 4d). Such hysteresis behavior supports that changes in the slowly evaporating signals were likely the main reason for the observed variations of Cl^+/HCl^+ ratios at different T_v.

Drewnick et al. (2015) suggested that tungsten oxide chloride (WO_2Cl_2(*g*)) is detected in AMS spectra from the interaction between sampled chloride aerosol species and vaporization surfaces, although signal levels are very small e.g., 0.04% of the total NH_4Cl signal. In this study, some ions consistent with WO_2Cl_2 signals, namely WCl^+ and WO_2^+ were also observed when sampling NH_4Cl with SV. The abundance of those ions was very low (< 0.02%), similar to Drewnick et al. (2015). Jimenez et al. (2003) reported MoO^+ and MoO_2^+ when sampling iodine-

Atmos. Meas. Tech. Discuss., doi:10.5194/amt-2016-337, 2016
Manuscript under review for journal Atmos. Meas. Tech.
Published: 9 November 2016

oxides with a prototype AMS vaporizer made of molybdenum. Following that work, we searched for the MoO^+, MoO_2^+, and $MoCl^+$ signals in the CV, but saw no detectable enhancement of either ion during NH_4Cl and other inorganic species sampling in this study.

NH_4 ions from NH_4NO_3, $(NH_4)_2SO_4$ and NH_4Cl

The abundance of NH_x^+ ions ($NH_x^+=NH^++NH_2^++NH_3^+$) from three NH_4-containing species (NH_4NO_3, $(NH_4)_2SO_4$ and NH_4Cl) vs T_v is shown in Fig. 4e-f. The fragmentation patterns of NH_4 across the different vaporizers and compounds were very similar. The fragmentation pattern of NH_4 in AMS was very consistent with the standard patterns of $NH_3(g)$ for 70 eV EI in the NIST database (Fig. 4e-f; Linstrom and Mallard, 2016). This strongly suggests that NH_x^+ ions in the AMS are mainly produced from direct EI ionization of evaporated $NH_3(g)$. A stable fragmentation pattern of NH_4 as a function of T_v (with variations of those abundances smaller than 4%) also suggests that thermal decomposition played a very minor role after $NH_3(g)$ evaporation.

3.1.4 Effect of particle beam position on the vaporizer

A key component of the AMS is an aerodynamic lens that focuses particles into a very narrow beam that is focused onto the center of the vaporizer (Liu et al., 1995a; Liu et al., 1995b; Jayne et al., 2000). The alignment of the particle beam onto the vaporizer center (typically referred to as “lens alignment”) is checked regularly, as mis-alignment can lead to particle losses and underestimation of particle concentrations. Lens alignment is usually performed with 300 nm pure NH_4NO_3 since these particles are know to be well focused (~0.5 mm beam diameter at the vaporizer) and a CPC is used to verify stable particle concentration during sampling (typically within 5% during an experiment). The lens position is varied (first horizontally, and later vertically, or vice versa), and the edges of vaporizer can be identified by a steep variation in

Atmos. Meas. Tech. Discuss., doi:10.5194/amt-2016-337, 2016
Manuscript under review for journal Atmos. Meas. Tech.
Published: 9 November 2016

aerosol signal. A microcalliper is used to read the lens position during this movement. In a CV AMS, lens alignment requires greater precision, since the entrance of the vaporizer is narrower than for SV (Fig. 1a). Lens alignment effects on signal intensity, fragmentation patterns, and size distributions of NH_4NO_3 for both vaporizers are discussed below. Since the cross section of vaporizer is radially symmetrical, lens alignment result from horizontal and vertical directions are generally very similar. Hence, only data from the horizontal dimension are shown (Figs. 5-6).

For these experiments, the lens was first aligned such that the particle beam almost missed the vaporizer on the left side and low NO_3 signal was observed. Then the particle beam was moved stepwise toward the edge of the vaporizer, which was identified by the sharp increase of NO_3 signal, then to the center of vaporizer, and finally to the other edge. For both vaporizers, the NO_3 signal shows a symmetrical variation with a broad plateau in the center (Figs. 5-6). In the CV, low NO_2^+/NO^+ is observed in the vaporizer center (~0.07) as previously-discussed (Fig. 3a). However, a much higher NO_2^+/NO^+ ratio (0.6-0.8) was observed at the edges of the vaporizer (Fig. 5). Those values are similar to those observed for SV (0.29-0.75). This is likely caused by the lack of many wall collisions for vapor molecules inside of the CV when the particle beam hits the CV edge, as illustrated in Fig. 1a. This enhanced NO_2^+ ion signal on the edge of vaporizer can also be used to detemine the center of lens alignment. When the beam is off the outside edge of the vaporizer assembly a small signal can still be observed since the particles impact on another surface (the vaporizer mount) just outside of the ionization chamber.

In the CV, the total nitrate signal also showed two peaks at the edge positions, 10-20% higher than at the center. The slightly higher NO_3 signal on the edge of CV may be due to a higher IE_{NO3} resulted from the different spatial distribution of vapor molecules, which may better overlap the electron beam and ion extraction regions or a different RIE of the particle vapor

Atmos. Meas. Tech. Discuss., doi:10.5194/amt-2016-337, 2016
Manuscript under review for journal Atmos. Meas. Tech.
Published: 9 November 2016

resulting from a change in thermal decomposition products on the vaporizer. E.g., at the edge the $HNO_3(g)$ fraction may be higher than at the center. $HNO_3(g)$ has a higher cross section due to its higher molar weight than $NO_2(g)$ and $NO(g)$ (and possibly a lower velocity), thus may result in more ions being formed. The higher NO_3 signal on the right edge vs left edge may be due to the right side being closer to the heated filament that supplies electrons for the ionization process, thus resulting in slightly larger overlap with the electron cloud and increasing ionization efficiency. Supporting this hypothesis, equal enhancement of NO_3 signal on the edges was observed for lens alignment in the vertical direction (not shown). In the SV, we did not observe this enhanced nitrate signal on the vaporizer edge (Fig. 6), which is consistent with the smaller difference in NO_2^+/NO^+ between vaporizer center and edge and the fact that hitting the center vs the edge of the SV is not expected to greatly change the number of vapor-wall collisions.

In contrast to the variable NO_2^+/NO^+, NH_2^+/NH^+ and NH_3^+/NH^+ from NH_4 did not show systematic differences between the center and the edge of both vaporizers. The constant ratios support direct EI ionization on $NH_3(g)$ as discussed above. Sightly lower RIE_{NH4} are observed at the edges of the CV due to higher nitrate signal and constant NH_4 signal. In the SV, RIE_{NH4} do not show systematic differences between the center and edges.

The size-resolved detection of NO_2^+, NO^+, NH_2^+ and NH_3^+ at the edge and center of both vaporizers are shown in Fig. 7, which was achieved by using PToF acquisition mode in the AMS. The measured PToF times represent both the actual (size dependent) particle velocity plus the vaporization and detection process. In these experiments particles of 300nm NH_4NO_3 were size selected using a DMA. At the edge of the CV, all ions peaked at the same time (Fig. 7a), while in the center the rise time of different ions was in the order: $NO_2^+ < NH_2^+/NH_3^+ < NO^+$ (Fig. 7b). The different rise time likely reflects increasing residence time of each precursor vapor

Atmos. Meas. Tech. Discuss., doi:10.5194/amt-2016-337, 2016
Manuscript under review for journal Atmos. Meas. Tech.
Published: 9 November 2016

in the CV cavity, presumably due to increasingly strong interactions with the surface. The same qualitative trend can in fact be observed for tails in the SV in Fig. 7a. The peak time when the particle beam hits the center of CV is 200 µs or more later than when hitting the CV edge. This delay represents a rough desorption and escape time for vapors from the CV cavity. In the SV, consistent peak times were observed at all vaporizer target positions, supporting that the delayed peak time at the center of CV is due to trapping in the cavity. The measured PToF times when impacting the edge of the CV are narrow as those from the SV. Thus, changing the lens alignment to focus particles on the CV edge can be used to obtain higher resolution size distributions in the CV for more volatile species, although presumably with degraded quantification of the total concentration.

3.1.5 Production of CO_2^+ from inorganic species

Pieber et al. (2016) have recently shown that CO_2^+ can be produced on the surface of the SV while sampling inorganic particles, presumably from the oxidation/decomposition and release of vapors from residual carbonaceous material on the vaporizer. This causes an interference in the quantification of organic species, which needs to be corrected by adjustments to the fragmentation table. The reported mass ratio (nitrate equivalent mass, i.e. using RIE=1) of the CO_2^+ produced vs the inorganic anion followed the order: $(NH_4)_2SO_4$ (0.1-0.3%) < NH_4NO_3 (~1%) < $NaNO_3$ (3-11%). Here we investigate this issue for the CV.

The CO_2^+ signal observed when sampling NH_4NO_3 in both vaporizers is shown in Fig. 8a. Those data were obtained after 4 days of exposing both AMSs to 10-1000 µg m^{-3} of SOA generated during chamber experiments, which could enhance this interference. Similar to Pieber et al. (2016), a CO_2^+/nitrate mass ratio (RIE=1 were applied to both) of 1.5% was observed for the SV (vs 0.7% before exposure). In contrast, negligible CO_2^+ was observed for the CV. We

Atmos. Meas. Tech. Discuss., doi:10.5194/amt-2016-337, 2016
Manuscript under review for journal Atmos. Meas. Tech.
Published: 9 November 2016

Atmospheric Measurement Techniques Discussions

further investigated this effect as a function of T_v (200-800℃; Fig. 8b). Negligible CO_2^+ (CO_2^+/nitrate < 0.4%) was observed for the CV over the entire T_v range, whereas in the SV ratios of ~1.2% were observed below 450℃ and increased ratios up to 3% were observed at 700-750℃. The negligible CO_2^+ formation from NH_4NO_3 in the CV may be due to the difference in thermal decomposition pathways between the CV and SV. As discussed above, the main product of nitrate in the CV is likely NO(*g*), which is not an efficient oxidizer as compared to NO_2(*g*) (Pieber et al., 2016). Difference in the vaporizer materials might also play a critical role as molybdenum is more inert than tungsten (Xu et al., 2016) and may highlight the different catalytic properties of the metals. CO_2^+/NO_3 ratios based on lens alignment are shown in the Figs. 5-6. No dependence of CO_2^+/NO_3 ratios in the SV with lens alignment was found (Fig. 6). However, in the CV, the CO_2^+/NO_3 ratios are a little higher at the vaporizer edge (Fig. 5), which is consistent with high NO_2^+/NO^+ ratio there.

However, when sampling $NaNO_3$ particles, CO_2^+ formation was observed in the CV (Fig. 8b). Two experiments were conducted, one with a "cleaner" CV (sampling little to no organic aerosols for days) and the other ("dirty") was done the next day after exposing the CV to 10-1000 µg m^{-3} of SOA from chamber studies for four days ("dirty" CV). For the cleaner CV, CO_2^+/nitrate for $NaNO_3$ (0.3-1.2%) was lower than for SV (1.2-12%), especially below 400℃. For the dirty condition, high ratios were observed above 500℃ for the CV (4-11%) and above 700℃ for the SV (4-9%). The CO_2^+ artifact in the CV from $NaNO_3$ (but not NH_4NO_3) might be due to substantial NO_2(*g*) formation from $NaNO_3$ thermal decomposition (e.g., $NaNO_3(s) \rightarrow NaO(s)+NO_2(g)$). The substantially enhanced CO_2^+ at T_v below 400℃ in the SV (Fig. 8b) corresponds to very enhanced NO_2^+/NO^+ ratios at lower T_v (shown in Fig. 4b and

Atmos. Meas. Tech. Discuss., doi:10.5194/amt-2016-337, 2016
Manuscript under review for journal Atmos. Meas. Tech.
Published: 9 November 2016

discussed below), which again supports the hypothesis of oxidation by $NO_2(g)$ reported by Pieber et al. (2016).

3.2 **CE of standard inorganic species**

CE of four inorganic species (NH_4NO_3, $(NH_4)_2SO_4$, $NaNO_3$ and NH_4Cl) in the CV is investigated here. The ratio of the mass concentrations of monodisperse particles as calculated for the AMS (using CE = 1) and CPC concentrations are shown in Fig. 9 as a function of T_v. To our knowledge, this is the first time that AMS CE has been reported as a function of T_v. All the AMS/CPC ratios (interpreted as CE), were calculated based on the IE and RIE obtained at 550-600℃. Field results suggest that RIE is not a strong function of temperature in the 350-600℃ range (Jimenez et al., 2016). Particle sizes of 250-300 nm were used to avoid particle losses by any other mechanism than bounce at the vaporizer (Huffman et al., 2005; Liu et al., 2007; Bahreini et al., 2008). However, d_m = 300 nm (mobility diameter) of $NaNO_3$ corresponds to d_{va} ~680 nm (= d_m × material density), which inadvertently exceed the size range of 100% lens transmission (d_{va}~550 nm for a well-functioning standard lens, e.g., Knote et al., 2011). Thus a correction factor is required for correction of the $NaNO_3$ data for lens transmission losses, so that the corrected ratio can be interpreted as CE due to vaporizer bounce only. Based on the measured lens transmission curves for the instruments used in this study (Fig. S2), lens transmissions fraction E_L = 0.6 and 0.8 were applied to the AMS/CPC ratio of 300 nm $NaNO_3$ in the SV and CV, respectively. No lens transmission corrections are needed for the other species.

NH_4NO_3

The AMS/CPC nitrate mass ratio vs T_v is shown in Fig. 9a1. An average ratio of 1±0.07 (avg.±stdv; range: 0.89-1.12) between T_v = 200-750℃ was observed for the SV. The variation of

Atmos. Meas. Tech. Discuss., doi:10.5194/amt-2016-337, 2016
Manuscript under review for journal Atmos. Meas. Tech.
Published: 9 November 2016

AMS/CPC ratios at other T_v compared to 600℃ (< 12%) was consistent with the reported 10% variation in AMS response to ambient particles as T_v was rapidly varied (Docherty et al., 2015). The AMS/CPC ratios of NH_4NO_3 in the SV did not show a clear trend with T_v. The ratio of background signal ("closed" particle beam) to aerosol input (CPC mass) was small, and exhibited a continuous decrease (0.12 to 0.04) with T_v, presumably due to somewhat slower evaporation at lower T_v.

In the CV, the AMS/CPC ratio of NH_4NO_3 was approximately 1 between 300-700℃, with lower ratios (~0.6-0.8) at extreme T_v (T_v < 300℃ or T_v > 700℃). The decreased AMS/CPC ratio at low T_v may be ascribed to slower evaporation. Similar to the SV, this was supported by a larger closed signal at lower T_v, e.g., ~0.12 at 200℃ vs ~0.005 at 500℃. Possible reasons for the decrease at the highest T_v (> 700℃) are stronger interactions of the analytes with the hot vaporizer surfaces, which is supported by a slightly higher nitrate closed signal is observed at high T_v, and/or a faster molecular speed reducing the effective ionization efficiency. To further examine this question, we study the aerosol signal decay and rise upon blocking and unblocking the particle beam (Fig. 10).

During typical MS mode operation, the beam-open and beam-blocked (closed) positions are alternated every several secs (usually ~5 s). During the particle beam modulation experiments, those intervals were extended to much larger values, typically 5-10 min of each, to allow studying the signal response at much longer times, similar to the study performed by Drewnick et al. (2015). The time resolution used was 1-3 s. Three T_v spanning the usable range (200℃, 600℃ and 850℃) were selected to perform the experiments in both vaporizers, as shown in Fig. 10. For the medium T_v = 600℃, rapid increase and decrease of nitrate signal (τ < 1s) was observed in both vaporizers. τ is defined here as the lifetime of signal decay when closing the particle beam

Atmos. Meas. Tech. Discuss., doi:10.5194/amt-2016-337, 2016
Manuscript under review for journal Atmos. Meas. Tech.
Published: 9 November 2016

after a long period of exposure to incoming particles. It was estimated through an exponential fit to the relevant part of the signal time series. τ for the signal rise after a long period without particles impacting the vaporizer is not shown, since it varies in the same way. After blocking the particle beam, the nitrate signal decreased to 8% of the beam-open signal after 3 s in the SV and to 1% after 1 s in the CV. Slower decays were observed at lower T_v = 200℃, namely 16% of open signal in the SV (3 s) and 24% in the CV (2 s), respectively. A slower rise of the nitrate signal at T_v = 200℃ was also observed in the CV upon unblocking the particle beam, which resulted in a lower open signal detection in the conventional MS mode (where the beam would be blocked again after a few seconds). Thus this experiment indicates that slower evaporation of nitrate at lower T_v indeed was the reason for the lower nitrate signal detected in the CV of AMS. At the higher T_v of 850℃, a faster decay of nitrate signal (3% of open signal in 3 s) than at 600℃ (8%) was observed in the SV. In the CV, beam-blocked signal remained elevated (~20% of open signal) and constant for the rest of beam-blocked time (~5 min). This difference in the background signal at higher T_v (> 700℃) indicates stronger interactions between the species decomposing from nitrate and the hot vaporizer surfaces.

$NaNO_3$

AMS/CPC ratios for $NaNO_3$ are shown in Fig. 9b. As T_v increases from 200℃ to 700℃, AMS/CPC ratios of $NaNO_3$ in SV increased dramatically (from 0.02 to ~0.85), indicating much improved detection of $NaNO_3$ at higher T_v (> 500℃). When T_v was above 550℃, the nitrate decay timescale was less than 2 s (beam-blocked = 7% of beam-open at T_v = 600℃), indicating that evaporation was fast enough for nitrate detection from $NaNO_3$ in MS mode. The ratio of ~0.85 is indicative of minor or particle bounce for $NaNO_3$

Atmos. Meas. Tech. Discuss., doi:10.5194/amt-2016-337, 2016
Manuscript under review for journal Atmos. Meas. Tech.
Published: 9 November 2016

In the CV, AMS/CPC ratios of $NaNO_3$ showed a qualitatively similar positive trend with T_v. However, the ratio in CV increased at much lower T_v (300℃) than for SV (500℃), indicating better detection of less volatile species in the CV, presumably due to the increased residence time and reduced bounce (or higher probability of finally vaporizing after multiple collisions inside the CV, right). For the beam open/blocked experiment (Fig. 10), indeed much faster particle decay was observed in the CV (τ~1s at 310℃) than in the SV (τ~12s at 330℃) at these temperatures. Above 550℃, the ratio in both vaporizers leveled off at 0.8-0.95. The partial cause of the plateau of the AMS/CPC ratio for $NaNO_3$ at less than 1 in the CV is probably due to the uncertainty of particle lens transmission loss correction. A full capture of $NaNO_3$ (E_b = 1) in capture vaporizer was reported based on AMS internal light scattering data (counting individual particles) (Xu et al., 2016). Another possible reason that cause lower NO_3 detection efficiency is that a Jayne shape factor (similar to NH_4NO_3) might be needed to correct the $NaNO_3$ density (2.26 g cm^{-3}). Or possibly the RIE of nitrate from $NaNO_3$ might be slightly lower than from NH_4NO_3 due to their different vapor precursors. Compared to the theoretical ion balance (mole ratio = 1), mole ratios between detected Na and NO_3 in both vaporizers were very low (< 0.04) based on an assumed RIE of Na of 1. Na is a refractory species (probably exists as NaO after thermal decomposition) that cannot be fully evaporated on the vaporizer, and it might retain some of the nitrate in the vaporizer for longer period.

$(NH_4)_2SO_4$

Pure $(NH_4)_2SO_4$ is a less volatile species and has been reported to have an E_b of 0.2-0.4 (200 nm) in the SV at T_v = 600℃, when sampling at ambient RH below its deliquescence point (Allan et al., 2004a; Matthew et al., 2008), while dry mixed ammonium sulfate-organic ambient particles typically have E_b ~0.5 (Middlebrook et al., 2012). In this study, a positive dependence

Atmos. Meas. Tech. Discuss., doi:10.5194/amt-2016-337, 2016
Manuscript under review for journal Atmos. Meas. Tech.
Published: 9 November 2016

Atmospheric Measurement Techniques Discussions

of the AMS/CPC SO_4 ratio vs T_v was observed for the SV, increasing from 0.2 at T_v = 200℃ to 0.55 at T_v > 500℃ (Fig. 9c1). This increase is likely due to both a lower particle bounce fraction and also faster evaporation. The decay timescale of SO_4 after blocking the particle beam was 26 s at T_v = 310℃ and < 2.5 s at T_v = 850℃ (Fig. 11)

In the CV, AMS/CPC SO_4 ratios were reproducibly 0.7-0.8 at T_v = 400-700℃ (Fig. 11). Results from independent experiments at Aerodyne confirmed AMS/CPC ratios of dry $(NH_4)_2SO_4$ in the CV were less than 1 (Xu et al., 2016). The ~25% missing signal suggests that a small fraction of pure $(NH_4)_2SO_4$ particles might still bounce on the edge of CV or that they may still bounce out of the CV without evaporating inside CV cavity. However, compared to the ratios of ~0.2-0.55 in SV, pure $(NH_4)_2SO_4$ is more efficiently detected in the CV. The beam open/blocked comparison also showed a much faster decay of SO_4 in the CV than in the SV for similar T_v. e.g., τ < 2 s in the CV vs τ = 13s in the SV at T_v = 550-610℃. The reduced AMS/CPC ratios at lower T_v in both vaporizers were probably caused by slower evaporation of sulfate (slow rise and decay signal in Fig. 11) and/or enhanced particle bounce at low T_v. The reason for the decrease of AMS/CPC ratio at higher T_v (> 700℃) in the CV may be due to enhanced interactions with the hot vaporizer surfaces, as hypothesized above for nitrate. Enhanced beam-blocked signal was observed at high T_v (Fig. 9c2), as observed for NH_4NO_3 and $NaNO_3$.

NH_4Cl

As discussed above, chloride appears to be very sticky on the vaporizer/ionizer surface, and is only slowly removed from the AMS background (Drewnick et al., 2015). Thus instrument history (e.g., chloride sampled and/or recent T_v history) or setup (e.g., different dutycycles) may influence NH_4Cl detection.

Atmos. Meas. Tech. Discuss., doi:10.5194/amt-2016-337, 2016
Manuscript under review for journal Atmos. Meas. Tech.
Published: 9 November 2016

Huffman et al. (2009) reported that NH_4Cl particles evaporated in a thermodenuder at higher temperature than NH_4NO_3 but lower than $(NH_4)_2SO_4$. However, the melting point/decomposition point of pure NH_4Cl is ~330℃ (Zhu et al., 2007), which is higher than those of $(NH_4)_2SO_4$ (235-280℃) (Haynes, 2015). AMS/CPC ratios of Cl from NH_4Cl (300 nm) in the SV were reproducibly 0.2-0.25, possibly due to the particle bounce and/or slow evaporation. High background signals and slow timescale of change were observed at all T_v for the SV (Figs. 9&11), consistent with the importance of the second hypothesis.

Slightly larger AMS/CPC ratios (0.27-0.35) were observed for the CV at T_v > 400℃. Two separate AMSs showed similar AMC/CPC ratios (0.33-0.37) at T_v = 550-600℃. The beam open/blocked experiment showed a faster chloride decay in the CV (τ = 5.2s) than the SV (τ =104s) at 550-600℃, mainly determined by the slower decaying Cl^+ ion (while the HCl^+ ion response was faster).

NH_4 from NH_4NO_3, $(NH_4)_2SO_4$ and NH_4Cl

For both SV and CV, the AMS/CPC ratios of NH_4 showed similar values and T_v dependences as their anions (Fig. 9). This is an indication that particle bounce played an important role for AMS/CPC ratios less than 1.

At medium T_v (500-650℃), NH_4 from the three species in both vaporizers all showed very low background (< 0.5%). In the beam open/blocked experiment, the decay lifetime of NH_4 was below 1-2 s, which was similar or faster than the anion decays. Despite of the lower background of NH_4, low AMS/CPC of NH_4 from $(NH_4)_2SO_4$ and NH_4Cl in both vaporizers was observed, strongly suggesting particle bouncing as the most likely explanation for the lower ratios of $(NH_4)_2SO_4$ and NH_4Cl observed in the CV as well.

Atmos. Meas. Tech. Discuss., doi:10.5194/amt-2016-337, 2016
Manuscript under review for journal Atmos. Meas. Tech.
Published: 9 November 2016

At lower T_v (< 350°C), NH_4 from the three inorganic species in the SV showed similar decay lifetime (< 2s) at medium T_v (500-650°C) and was much faster than their anion decays (2-184s). NH_4 decay in the CV at low T_v (~200-330°C) exhibited a τ ~16s for NH_4NO_3, ~2s for $(NH_4)_2SO_4$ and 10s for NH_4Cl, which was longer than NH_4 in the SV under similar low T_v range. The longer NH_4 decay suggested slower release of $NH_3(g)$ in the CV than the SV at this low T_v range (< 350°C), perhaps due to stronger surface interactions. The NH_4 decay in the CV was still faster than their anions of SO_4 and Cl, which may explain why AMS/CPC ratios of NH_4 were higher than SO_4 and Cl and anion/cation ratios (0.2 to 1) decreased at lower T_v (400°C; Figs. 9b2-3 and d2-3). At higher T_v, AMS/CPC ratios of NH_4 exhibited similar ratios to their anions. A small background enhancement at higher T_v in the CV was also observed.

Implications for evaporation mechanisms in the AMS

It has recently been suggested that NH_4NO_3 and $(NH_4)_2SO_4$ evaporate as intact salts in the AMS (Murphy, 2016). The stability of the ammonium fragmentation pattern across temperatures and vaporizers and their similarity to the NIST spectrum for $NH_3(g)$ (Linstrom and Mallard, 2016), combined with the substantial variations observed for sulfate and nitrate (section 3.1.4), strongly contradict that possibility. The different decay times of NH_4 and their anions after blocking the particle beam (Figs. 10-11) also supports that thermal decomposition, followed by separate interactions with hot surfaces, is an important step in particle detection in the AMS. Thus NH_4NO_3, $(NH_4)_2SO_4$ and NH_4Cl do not appear to evaporate as intact gas molecules (e.g., $NH_4NO_3(g)$), but to mainly undergo thermal decomposition to liberate $NH_3(g)$ and the acid vapor [$HNO_3(g)$ or $H_2SO_4(g)$ or $HCl(g)$] or other species first before ionization in the AMS (Drewnick et al., 2015; Jimenez et al., 2016). The acid vapor, in particular, $HNO_3(g)$ or $H_2SO_4(g)$, can undergo further thermal decomposition.

Atmos. Meas. Tech. Discuss., doi:10.5194/amt-2016-337, 2016
Manuscript under review for journal Atmos. Meas. Tech.
Published: 9 November 2016

Atmospheric Measurement Techniques Discussions

3.3 **Size distribution measurements**

3.3.1 Size-resolved detection of ions at T_v~ 500-650℃

The determination of particle size distributions in the AMS is based on measuring size dependent particle flight times, or PToF, which are on the time scale of milliseconds. A pre-requisite to precise size distribution determinations is rapid particle vaporization and detection times, which need to be much faster than the millisecond PToF time scale, ideally 10s of microseconds. When the rates of vaporization and/or decomposition are reduced, the resolution of the AMS sizing is also reduced. This is a more stringent requirement than quantifying the total mass concentrations in MS mode which only require evaporation and detection to be on the order of ~5s where the particle beam is alternately blocked or sampled. In this section we evaluate the ability to measure size distributions with the CV. Results from the inorganic species $(NH_4)_2SO_4$, NH_4NO_3, $NaNO_3$, as well as of organic nitrates generated from NO_3 radical + monoterpene chamber studies are discussed below (Fig. 12).

Generally, ions from each species showed similar rise times in the SV (~100 µs, Fig. 12), indicating aerosols were quickly evaporated and detected after impact on the open SV surface. Compared to the SV, most PToF distributions in the CV exhibited a slower rise, and larger differences for different ions/species. Although that will lead to lower sizing resolution, it clearly shows that size distributions can still be measured with the CV. The earlier rise of NO_2^+ than NO^+ in inorganic nitrates in the CV may be due to reduced surface interactions of $HNO_3(g)$ and $NO_2(g)$ (which can yield NO_2^+ ions) than for $NO(g)$. In contrast to inorganic nitrates, NO_2^+ from organic nitrates showed a delayed tail vs NO^+. This tail has also been seen in the CV for other organic nitrates from NO_3 radical + monoterpene chamber studies, and might be a useful approach to identify and quantify organic nitrates (e.g., Fry et al., 2013) when using the CV.

Atmos. Meas. Tech. Discuss., doi:10.5194/amt-2016-337, 2016
Manuscript under review for journal Atmos. Meas. Tech.
Published: 9 November 2016

NH_4 from inorganic species in the CV showed a slightly earlier rise than NO^+ and SO_2^+/SO^+ (Fig. 12e and f). This may be associated with faster vaporization of $NH_3(g)$ and faster effusion out of the CV due to its lower molecular weight and reduced surface interactions. The faster detection of NH_x^+ in the CV also supports the conclusion that NH_4NO_3 and $(NH_4)_2SO_4$ salts mainly thermally decomposed before ionization (Drewnick et al., 2015). Thermal decomposition is particularly evident from Fig. 12e where it is seen that the NO_2^+ ion fragment is vaporized and detected on a faster time scale than the NH_x^+ and NO^+ ion fragments in the CV compared to the SV.

3.3.2 Distribution as a function of temperature

PToF distributions of monodisperse particles from three standard species ($(NH_4)_2SO_4$, NH_4NO_3 and $NaNO_3$) in both vaporizers as a function of T_v are shown in Fig. 13a-b. Figure 13c is a summary of FWHM as a function of T_v based on Fig. 13a-b. In the following discussion, three different aspects including transition T_v, peak broadening, and PToF vs MS mode are discussed. The PToF distribution of each species reported is the sum for all its ions, and thus is a convolution of slightly different behaviors from each ion, as shown e.g. in Fig. 12.

(1) *Transition T_v ($T_{v,t}$)* is defined as the T_v above which particles show a narrow distribution (< 1 ms for nitrate and sulfate in the SV, 2 ms for sulfate in the CV). Above this T_v, stable peak shapes and similar peak widths are typically observed (Fig. 13a3-c3). $T_{v,t}$ appears to be mainly a function of species volatility with values for NH_4NO_3 (~280℃) < $(NH_4)_2SO_4$ (380℃) < $NaNO_3$ (~630℃) in the SV. This sequence is similar to the reported melting point trends for those species: NH_4NO_3:169℃ < $(NH_4)_2SO_4$: 235-280℃ < $NaNO_3$: 306℃ (Haynes, 2015), as well as their boiling points, as shown in Fig. 14. Similar positive trends were also observed in the CV, where $T_{v,t}$ of NH_4NO_3 and $(NH_4)_2SO_4$ in the CV

Atmos. Meas. Tech. Discuss., doi:10.5194/amt-2016-337, 2016
Manuscript under review for journal Atmos. Meas. Tech.
Published: 9 November 2016

were similar for NO_3 (~200℃) and SO_4 (370℃) with the SV, and $T_{v,t}$ of $NaNO_3$ is slightly lower than the SV (630℃). The lower $T_{v,t}$ of $NaNO_3$ was probably due to longer residence time and more collisions between particle and vaporizer heating surfaces in the CV. NH_4 from NH_4NO_3 in the CV show a high $T_{v,t}$ (380℃) than in the SV (280℃). The slower evaporation of NH_4 than NO_3 for the CV at low T_v was also observed in the beam open/blocked experiment (Fig. 10).

The linear relationship between $T_{v,t}$ and melting/boiling points probably could be used for estimating whether pure species are detected in AMS sizing mode. E.g. the anion of $NaNO_3$ or species with lower than or similar melting points to $NaNO_3$, e.g., $MgNO_3$ (129℃) or KNO_3 (334℃), can likely be detected and quantified by the CV at 600℃ in both MS and PToF modes. Further research on less-volatile species detection in the CV AMS, as well as the correlation of their fast detection T_v with melting and boiling points is recommended.

The peak widths of NH_4NO_3 (both NH_4 and NO_3) at higher T_v (> 700℃) start to broaden in the CV, which may be indicative of increased surface interactions as discussed above.

(2) *Peak broadening in CV***.** For monodisperse particles, the peak width of AMS PToF distribution is primarily governed by thermal decomposition rates and rate of effusion of particle vapors to exit the CV (Drewnick et al., 2015). The latter mainly depends on T_v, interaction between particle and vaporizer surface, vaporizer design and molecular speeds. In the SV for $T_v > T_{v,t}$ (Fig. 13), the peak width of three species followed the order of $NH_4NO_3 < NaNO_3 < (NH_4)_2SO_4$, all within 1 ms.

Atmos. Meas. Tech. Discuss., doi:10.5194/amt-2016-337, 2016
Manuscript under review for journal Atmos. Meas. Tech.
Published: 9 November 2016

Atmospheric Measurement Techniques Discussions

Compared to the SV, PToF distributions in the CV showed broader peak widths, indicating longer vapor desorption/escape times. The peak width ratios between the CV and SV, defined as broadening ratios, vary widely between species: ~5.5 for $(NH_4)_2SO_4$, 2 for NH_4NO_3 and 1.8 for $NaNO_3$. The broadened peaks in the CV, leading to lower particle size resolution, degrades size distribution measurement in laboratory studies with monodisperse particles. E.g., a small double charged peak of $NaNO_3$, observed with the SV cannot be separated in the CV (Fig. 13c1-2). However, size distributions in ambient air tend to be broad, and thus the size distribution measurement in CV will still be useful.

(3) *Comparison of total detected signal in PToF vs MS mode.* As discussed above, the MS and PToF modes integrate detection timescales of ms and s, respectively. Thus the total signal ratio between PToF and MS modes can be used as an alternative tool to quantify the evaporation rates of different species, as shown in Fig. 14.

For NH_4NO_3, PToF/MS of both vaporizers at low T_v (200-400℃) showed a continuously increasing trend, consistent with faster evaporation and decomposition/desorption as T_v increased (Fig. 15a). PToF/MS ~1 for NO^+ and NO_2^+ was observed in both vaporizers for T_v = 450-700℃. For T_v > 650℃, the PToF/MS of NO^+ and NO_2^+ continuously decreased in the CV, suggesting a less efficient quantification from PToF than MS mode, in agreement with the broadened PToF peaks (Fig. 13c3) at those T_v. PToF/MS for $NaNO_3$ increased continuously until reaching 1 at 500℃ and 550℃ for the CV and SV, respectively (Fig. 15b), which is consistent with the PToF widths vs T_v (Figs. 13c1-c3). For sulfate (Fig. 15c), the PToF/MS ratio in both vaporizers increased with T_v between 300-800℃. This increase was mainly associated with faster evaporation/detection.

Atmos. Meas. Tech. Discuss., doi:10.5194/amt-2016-337, 2016
Manuscript under review for journal Atmos. Meas. Tech.
Published: 9 November 2016

Atmospheric Measurement Techniques Discussions

Based on all the T_v-dependent experiments discussed above, we recommend an operating T_v~500-550℃ for CV for normal usage. In this temperature range, fast evaporation of inorganic particles with high CE and reduced distortion of PToF distributions are observed, while fragmentation (including of organic species) is reduced and slower response effects observed at high T_v (e.g., > 700℃) can be avoided.

4 Conclusions

To reduce the quantification uncertainty of non-refractory aerosols due to particle bounce in the AMS, a CV has been designed with the goal of trapping particles inside the vaporizer body to achieve near unity collection efficiency thereby reducing one of the largest uncertainties associated with the AMS quantification which is particle bounce.

The performance of the CV was quantified and compared with the SV for four inorganic standard species NH_4NO_3, $NaNO_3$, $(NH_4)_2SO_4$ and NH_4Cl, representative of ambient nitrate, sulfate, ammonium and chloride species. The whole range of practical T_v (200-800℃) was explored. The main conclusions are:

1) Thermal decomposition is a key step in aerosol detection in the AMS. The fragmentation patterns of inorganic species in the CV shift toward smaller mass fragments compared with the SV. This shift is caused by a greater degree of thermal decomposition in the vaporizer due to the increased residence time of condensed and/or vapor phase molecules on the walls of the CV.
2) Multiple results support that NH_4NO_3, $(NH_4)_2SO_4$ and NH_4Cl do not evaporate as intact molecular species but first decompose to $NH_3(g)$ + $HNO_3(g)$ or $H_2SO_4(g)$ or $HCl(g)$ (and other anion product species). T_v enhances thermal decomposition of NO_3 and SO_4. The

Atmos. Meas. Tech. Discuss., doi:10.5194/amt-2016-337, 2016
Manuscript under review for journal Atmos. Meas. Tech.
Published: 9 November 2016

Atmospheric Measurement Techniques Discussions

HCl^+/Cl^+ and NH_x^+ ions show little dependence on T_v and thus appear to be mainly produced by ionization of HCl(*g*) and NH_3(*g*).

3) CE of NH_4NO_3, $NaNO_3$, $(NH_4)_2SO_4$ and NH_4Cl in the CV at 500-600℃ were ~1, ~0.95, ~0.8 and ~0.35, respectively, which were comparable or higher than those in the SV (~1, ~0.85, ~0.4, and ~0.25), indicating reduced particle bounce fraction in the CV. Although the CE of some pure inorganic species were still less than 1 in the CV, when mixed with organic and NH_4NO_3 in the ambient particles, they will likely have a higher CE, as it is observed for e.g. ambient $(NH_4)_2SO_4$ in the SV (e.g. Middlebrook et al., 2012). This will be investigated with field data in the future.

4) In this study, we found a temperature-dependent trend of the mass ratio between CO_2^+ produced and NO_3 sampled in the SV (1-10%) likely due to catalytic reactions liberating charred carbon on the vaporizer. In the CV, negligible CO_2^+ (< 0.4%) was formed when sampling NH_4NO_3 particles. $NaNO_3$ particle in the CV can produce comparable amount of CO_2^+ per NO_3 mass to the SV (up to 10%) when the CV has been recently exposed to high level of OA. In ambient air with typically negligible or very small submicron $NaNO_3$ concentrations, this CO_2^+ artifact should much smaller than for the SV, and thus much less an interference for OA concentration and properties. It could also improve organic CO_2 quantification in source studies where ammonium nitrate >> OA (such as chamber studies with vehicle exhaust, Pieber et al., 2016).

5) The PToF distributions of species measured using the CV are broadened, which will reduce the size resolution. This effect will be most important for laboratory experiments with monodisperse particles. For ambient air with typically broad size distributions, size distributions measured from an AMS using the CV are expected to be useful. A method

for estimating whether a pure species can be detected by the AMS sizing mode at a given T_v is proposed.

6) Particle-beam position-dependent results showed that particle detection with the CV resembles the detection with the SV for NH_4NO_3, when the particle beam is focused on the edge of CV. Minimal distortion in the PToF measurement can be achieved under that condition. For practical usage, this setup may be useful to increase size resolution in laboratory studies with monodisperse particles. Whether this benefit extends to less-volatile species should be investigated in future studies.

7) Based on all the results of T_v-dependent experiments, a T_v ~500-550℃ for the CV is recommended.

Acknowledgements

This study was partially supported by NSF AGS-1360834, NASA NNX15AT96G, DOE (BER/ASR) DE-SC0011105, DE-SC0016559, NOAA NA13OAR4310063 and DOE Small Business Innovative Research (SBIR) contract #DE-SC0001673. We sincerely thank Melissa Ugelow, Hyungu Kang, Jason Schroder and Benjamin Nault of CU-Boulder for support in specific experiments.

Atmos. Meas. Tech. Discuss., doi:10.5194/amt-2016-337, 2016
Manuscript under review for journal Atmos. Meas. Tech.
Published: 9 November 2016

Atmospheric Measurement Techniques Discussions

Table 1. Fragmentation patterns of particulate nitrate from NH_4NO_3 particles and particulate sulfate from $(NH_4)_2SO_4$ particles. Both fragmentation patterns were measured in pure argon gas. The intensity relative to the largest peak and the fraction of total are reported. The uncertainties of the fragment fractions correspond to the variability of the data as one standard deviation.

	Mass	Fragment		Rel. intensity			Fraction (%)		
UMR Mass	HR Mass	Ions[a]	Parent ions	CV[b]	SV[b]	SV Lit.[c]	CV[b]	SV[b]	SV Lit.[c]
					NH_4NO_3				
30	29.9980	NO^+	NO^+	100.00	100.00	100.00	92.46±1.06	72.86±3.81	56.49±4.64
46	45.9929	NO_2^+	NO_2^+	7.47	34.78	74.93	6.90±1.05	25.35±4.29	42.23±8.04
63	62.9956	HNO_3^+	HNO_3^+	0.07	0.90	0.86	0.07±0.03	0.66±0.05	0.49±0.11
					$(NH_4)_2SO_4$				
16	15.9949	O^+	O^+	6.09	8.56	0.70	2.02±0.22	2.14±0.55	0.18±0.01
17	17.0027	HO^+	HO^+	20.85	22.91	16.80	6.92±0.58	5.72±0.19	4.25±0.34
18	18.0106	H_2O^+	H_2O^+	91.06	100.00	78.16	30.22±0.93	24.96±0.62	19.75±1.58
24	23.9835	SO^{2+}	SO^+	0.49	0.59	0.62	0.16±0.03	0.15±0.02	0.16±0.02
32	31.9721	S^+	S^+	8.13	9.82	14.06	2.70±0.28	2.45±0.82	3.55±0.09
48	47.967	SO^+	SO^+	60.11	78.10	67.09	19.95±0.39	19.49±0.34	16.95±0.41
49	48.9748	HSO^+	HSO^+	0.01	0.44	N/A	<0.01	0.11±0.01	N/A
50	49.9826	H_2SO^+	H_2SO^+	<0.01	0.19	N/A	<0.01	0.05±0.02	N/A
64	63.9619	SO_2^+	SO_2^+	100.00	85.82	100	33.19±0.53	21.42±0.39	25.26±1.50
65	64.9613	$j^{33}SO_2^+$	SO_2^+	0.92	0.68		0.31±0.02	0.17±<0.01	
65	64.9697	HSO_2^+	HSO_2^+	0.23	6.10	5.69	0.07±0.01	1.52±0.05	1.44±0.17
80	79.9568	SO_3^+	SO_3^+	0.02	38.03	56.70	0.91±0.03	9.49±0.14	14.33±2.15
81	80.9562	$j^{33}SO_3^+$	SO_3^+	2.75	0.30		0.06±0.03	0.07±<0.01	
81	80.9646	HSO_3^+	HSO_3^+	0.17	23.77	26.23	0.40±0.03	5.93±0.16	6.63±0.53
82	81.9725	$H_2SO_3^+$	$H_2SO_3^+$	0.02	0.27	N/A	<0.01	0.07±0.03	N/A
96	95.9517	SO_4^+	SO_4^+	<0.01	<0.01	N/A	<0.01	<0.01	N/A
97	96.9418	$HS_2O_2^+$	$HS_2O_2^+$	<0.01	<0.01	N/A	<0.01	<0.01	N/A
97	96.9596	HSO_4^+	HSO_4^+	<0.01	0.06	N/A	<0.01	0.01	N/A
98	97.9674	$H_2SO_4^+$	$H_2SO_4^+$	0.12	12.55	16.7	0.25±0.03	3.13±0.06	4.22±0.51

[a] All the isotope ions are calculated based on isotope ratios in fragmentation table, thus not shown here, which account for ~1% of nitrate and ~3% of sulfate in the SV and ~0.5% of nitrate and ~3% in sulfate in the CV. [b] This study; [c] from Hogrefe et al. (2004).

Atmos. Meas. Tech. Discuss., doi:10.5194/amt-2016-337, 2016
Manuscript under review for journal Atmos. Meas. Tech.
Published: 9 November 2016

Atmospheric Measurement Techniques Discussions

Table 2. Fragmentation table for the AMS data analysis software, as modified for the CV based on $(NH_4)_2SO_4$ measurement in pure argon gas. The default settings in the analysis software for SV are also shown. These ratios should be implemented in both UMR and HR fragmentation table.

m/z/ion	Frag_sulfate	Frag_SO_3	
		SV (default)	CV
18/H_2O^+	Frag_SO_3[18]	0.67*frag_SO_3[64], 0.67*frag_SO_3[48]	0.56*frag_SO_3[64], 0.56*frag_SO_3[48]
32/S^+	Frag_SO_3[18], Frag_H_2SO_4[32]	0.21*frag_SO_3[64], 0.21*frag_SO_3[48]	0.05*frag_SO_3[64], 0.05*frag_SO_3[48]

Atmos. Meas. Tech. Discuss., doi:10.5194/amt-2016-337, 2016
Manuscript under review for journal Atmos. Meas. Tech.
Published: 9 November 2016

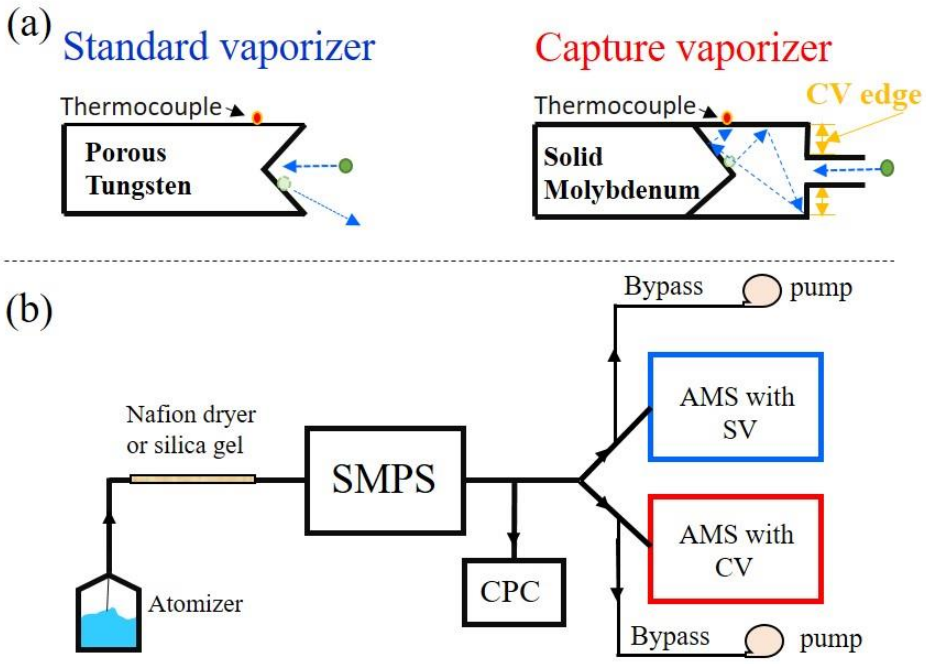

FIG. 1 (a) Schematic diagrams of the standard vaporizer (SV) and capture vaporizer (CV). More details of CV design can be found in Xu et al. (2016). The appearance of the SV and CV are shown in Fig. S1. (b) Setup of laboratory experiments for comparing the SV and CV. The sampling gas was kept at below 30% RH by Nafion dryers and/or silica gel diffusion dryers.

Atmos. Meas. Tech. Discuss., doi:10.5194/amt-2016-337, 2016
Manuscript under review for journal Atmos. Meas. Tech.
Published: 9 November 2016

Atmospheric Measurement Techniques Discussions

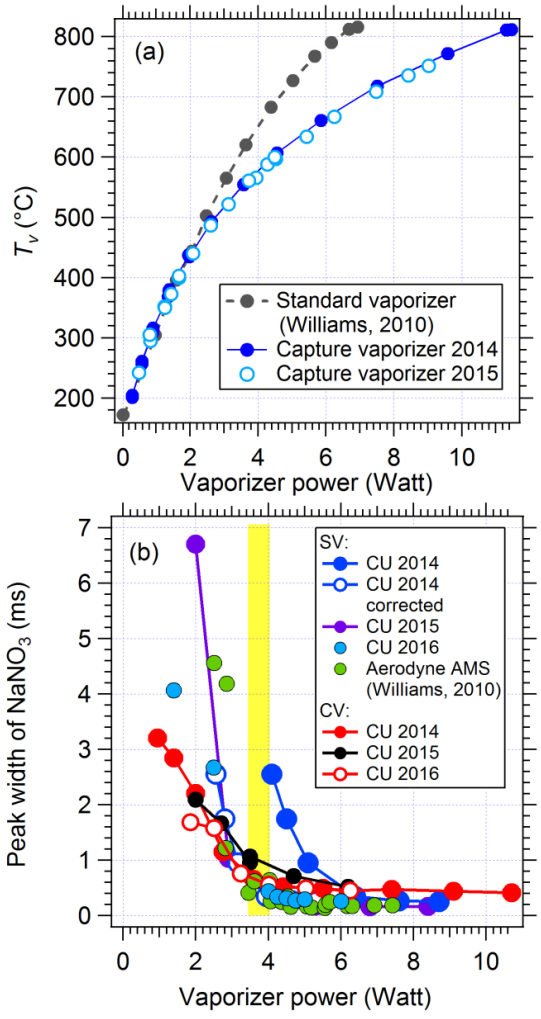

FIG. 2 (a) Relationship between vaporizer temperature (T_v, as reported by the attached thermocouple) and vaporizer power. (b) Peak width of measured size distributions of 300 nm $NaNO_3$ particles as a function vaporizer power. In Fig. 2b, the 2014 curve between peak width vs vaporizer power in the SV indicated that the vaporizer power reading in that AMS system was inaccurate during those tests (see main text). Therefore, a correction (*Corrected vaporizer power* = 0.6×*displayed vaporizer power*+0.1) was applied. The yellow background shows the range of vaporizer power between 3.6-4 W, which is a transition in the detected peak width observed in both vaporizers.

Atmos. Meas. Tech. Discuss., doi:10.5194/amt-2016-337, 2016
Manuscript under review for journal Atmos. Meas. Tech.
Published: 9 November 2016

Atmospheric Measurement Techniques Discussions

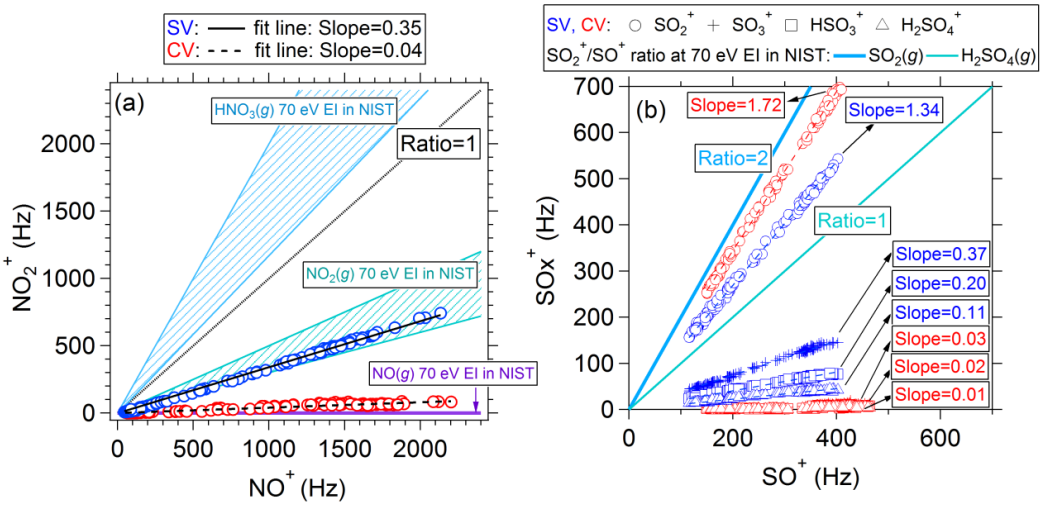

FIG. 3 Scatter plots of (a) NO_2^+/NO^+ for NH_4NO_3 and (b) SO_x^+/SO^+ for $(NH_4)_2SO_4$ measured with AMS with the SV and CV. NO_2^+/NO^+ ratios the NIST database for 70 eV EI ionization of $HNO_3(g)$, $NO_2(g)$ and $NO(g)$ are also shown in Fig. 3a. SO_2^+/SO^+ ratios from NIST for $SO_2(g)$ and $H_2SO_4(g)$ are also shown in Fig. 3b. SO_x^+ ions include SO_2^+, SO_3^+, HSO_3^+ and $H_2SO_4^+$.

Atmos. Meas. Tech. Discuss., doi:10.5194/amt-2016-337, 2016
Manuscript under review for journal Atmos. Meas. Tech.
Published: 9 November 2016

Atmospheric Measurement Techniques Discussions

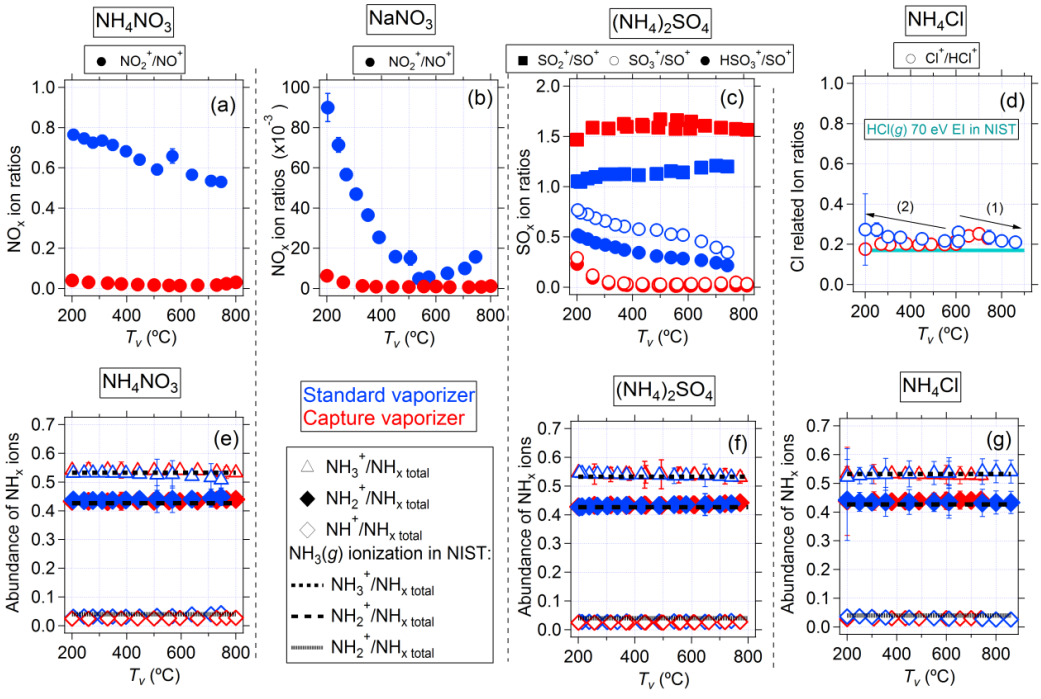

FIG. 4 Fragmentation patterns of pure inorganic standard species vs T_v for the SV and CV: (a) and (e) NH_4NO_3, (b) $NaNO_3$, (c) and (f) $(NH_4)_2SO_4$, and (d) and (g) NH_4Cl. Error bars are standard deviations. For the NH_4Cl experiment, we first increased T_v from 600℃ (arrow labeled 1) in both the SV and CV, then tune back to the 600℃, and decreased the T_v to 200℃ (arrow 2).

Atmos. Meas. Tech. Discuss., doi:10.5194/amt-2016-337, 2016
Manuscript under review for journal Atmos. Meas. Tech.
Published: 9 November 2016

Atmospheric Measurement Techniques Discussions

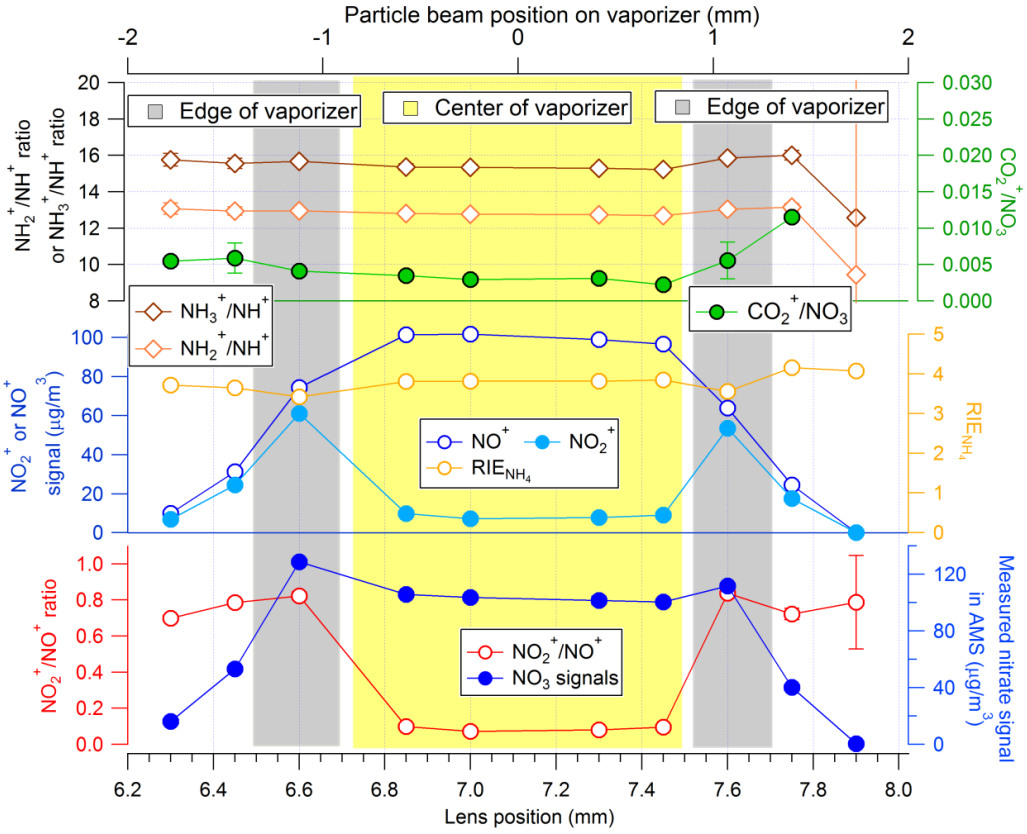

FIG. 5 CV: Particle beam position dependence of NO_2^+/NO^+, total detected nitrate, NO_2^+ and NO^+ signals, RIE of NH_4 (RIE_{NH4}) and nitrate equivalent mass ratio of CO_2^+/NO_3. The shaded areas are rough indication for where the particle beam hit the vaporizer. A constant IE obtained with pure NH_4NO_3 particle at the center of the lens was applied to all data collected in this experiment. The particle size-resolved detection for the edge and center positions are shown in Fig. 7.

Atmos. Meas. Tech. Discuss., doi:10.5194/amt-2016-337, 2016
Manuscript under review for journal Atmos. Meas. Tech.
Published: 9 November 2016

Atmospheric Measurement Techniques Discussions

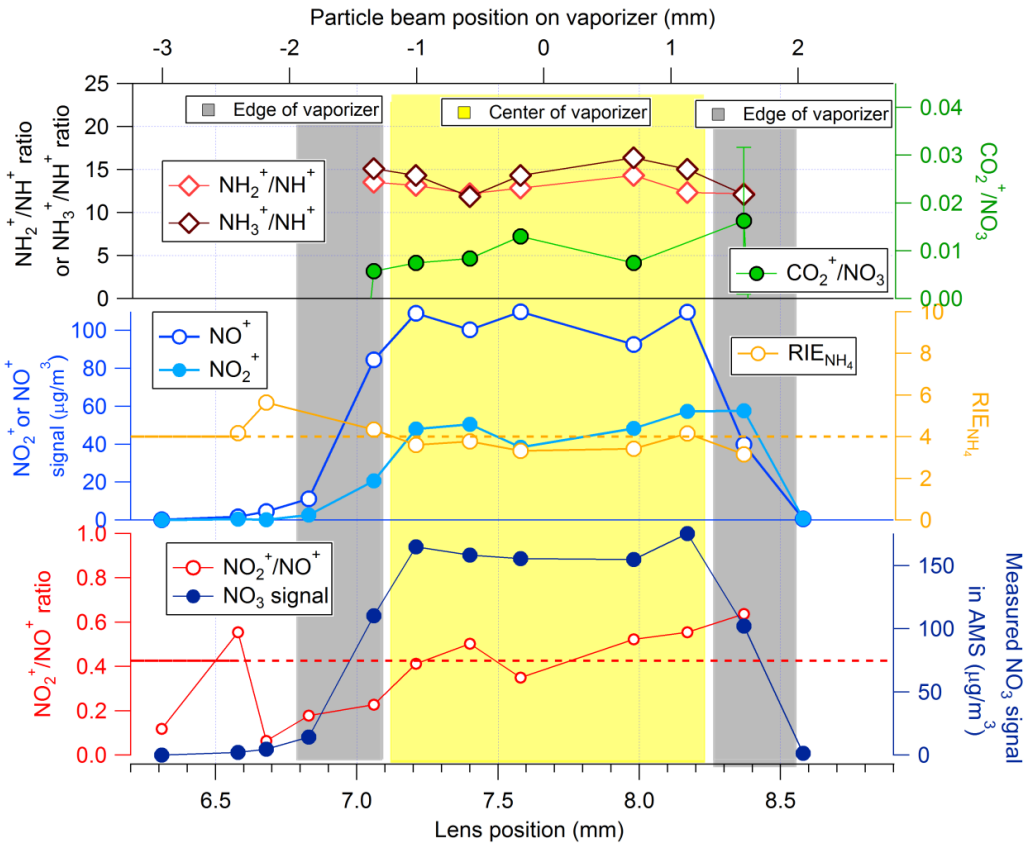

FIG. 6 SV: particle beam position dependence of NO_2^+/NO^+, total nitrate, NO_2^+ and NO^+ signals, RIE of NH_4 and nitrate equivalent mass ratio of CO_2^+/NO_3. The shaded areas are rough indication for where the particle beam hit the vaporizer. A constant IE obtained with pure NH_4NO_3 particle at the center of the lens was applied to all data collected in this experiment. The particle size-resolved detection for the edge and center positions are shown in Fig. 7.

Atmos. Meas. Tech. Discuss., doi:10.5194/amt-2016-337, 2016
Manuscript under review for journal Atmos. Meas. Tech.
Published: 9 November 2016

Atmospheric Measurement Techniques Discussions

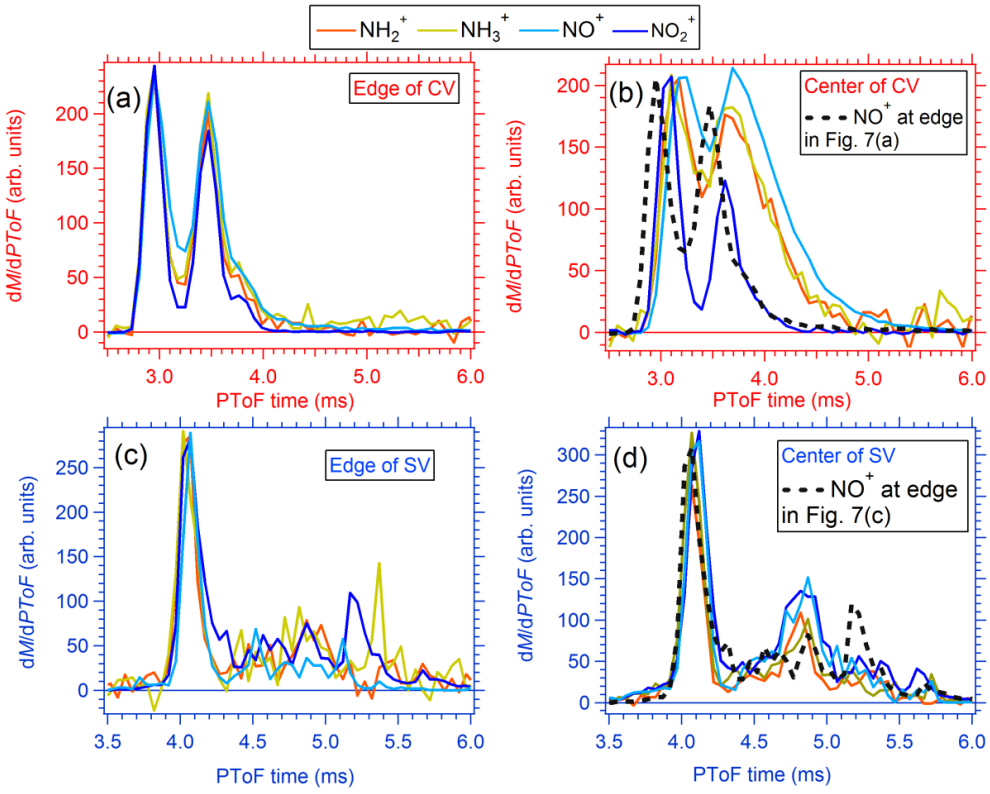

FIG. 7 Size-resolved detection of NH_4NO_3 (double charged 300 nm particles selected by DMA) major ions using the PToF acquisition mode at (a) CV edge (position = 7.6 mm), (b) CV center (position = 7.1 mm), (c) SV edge (position = 8.4 mm) and SV center (position = 7.9 mm). All the peaks were normalized to the NO^+ maximum. Note that the size distributions of the particles were identical within each panel, and that the differences observed between the different ions are due to evaporation and other effects. (see main text). The experiments for the SV and CV were performed at different times, and the fraction of doubly-charged particles was lower for the SV experiment.

Atmos. Meas. Tech. Discuss., doi:10.5194/amt-2016-337, 2016
Manuscript under review for journal Atmos. Meas. Tech.
Published: 9 November 2016

Atmospheric Measurement Techniques Discussions

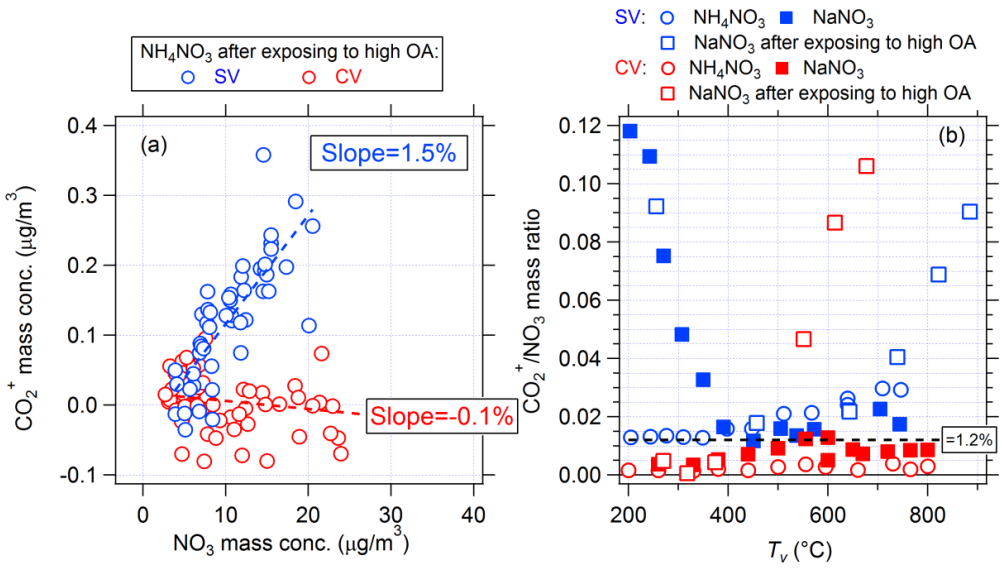

FIG. 8 (a) Scatter plots of CO_2^+ and particulate nitrate signals when pure NH_4NO_3 particles were sampled into two AMSs with a SV and CV, respectively. These data were collected after 4-days of exposing both AMS a wide range of SOA mass concentrations (10-1000 μg m^{-3}) from chamber studies. (b) Ratios of CO_2^+ to particulate nitrate vs T_v. All data are in nitrate-equivalent units. The data for $NaNO_3$ after exposing to OA were collected during a similar period as shown Fig. 4a, while the other $NaNO_3$ data were collected in a different period.

Atmos. Meas. Tech. Discuss., doi:10.5194/amt-2016-337, 2016
Manuscript under review for journal Atmos. Meas. Tech.
Published: 9 November 2016

Atmospheric Measurement Techniques Discussions

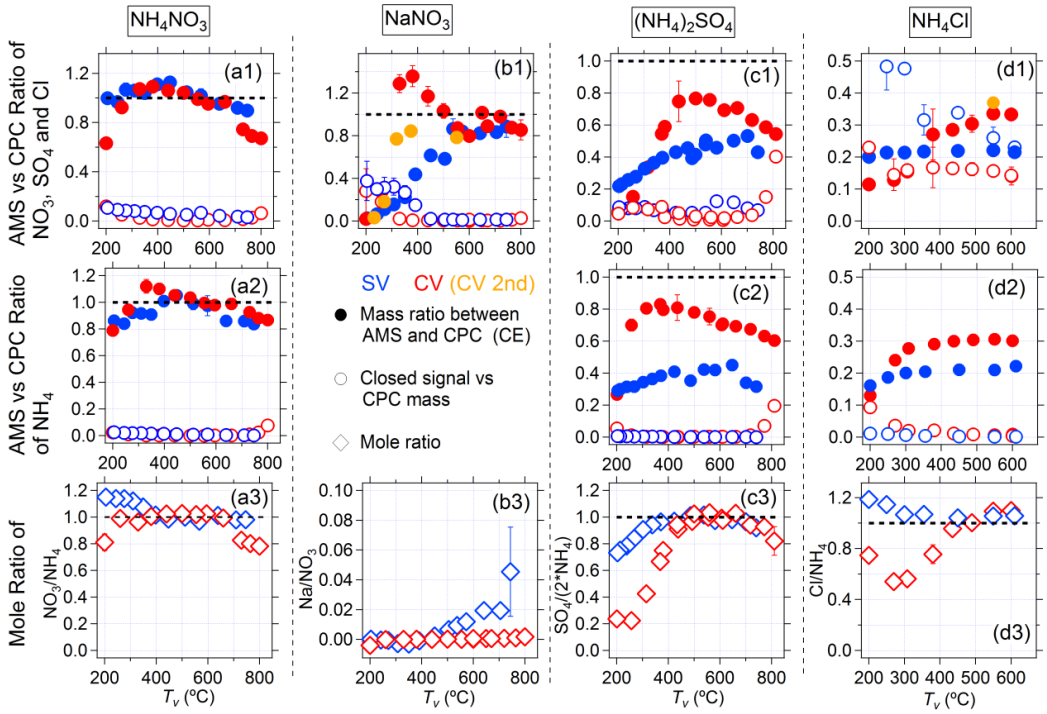

FIG. 9 Ratio of mass concentration between AMS and CPC measurements (CE) from four dry monodisperse particles of inorganic species (a) 300nm NH_4NO_3; (b) 250 nm $(NH_4)_2SO_4$; (c) 300 nm $NaNO_3$; (d) 300 nm NH_4Cl; as a function of T_v in SV and CV. Apparent mole ratios between anion vs cation (a3, c3 and d3) and cation vs anion (b3) are also shown (bottom row). The $NaNO_3$ AMS/CPC ratios were corrected with the lens transmission curve in Fig. S2 (see text). The orange traces in Fig. 9c1 and Fig. 9d1 are results from repeat CV experiments. The mole ratio of $(NH_4)_2SO_4$ is SO_4 vs $2NH_4$. RIE of sodium was assumed to be 1 here since no explicit RIE of Na has been reported to our knowledge, and since this species is both slow to evaporate and prone to surface ionization in the AMS.

Atmos. Meas. Tech. Discuss., doi:10.5194/amt-2016-337, 2016
Manuscript under review for journal Atmos. Meas. Tech.
Published: 9 November 2016

Atmospheric Measurement Techniques Discussions

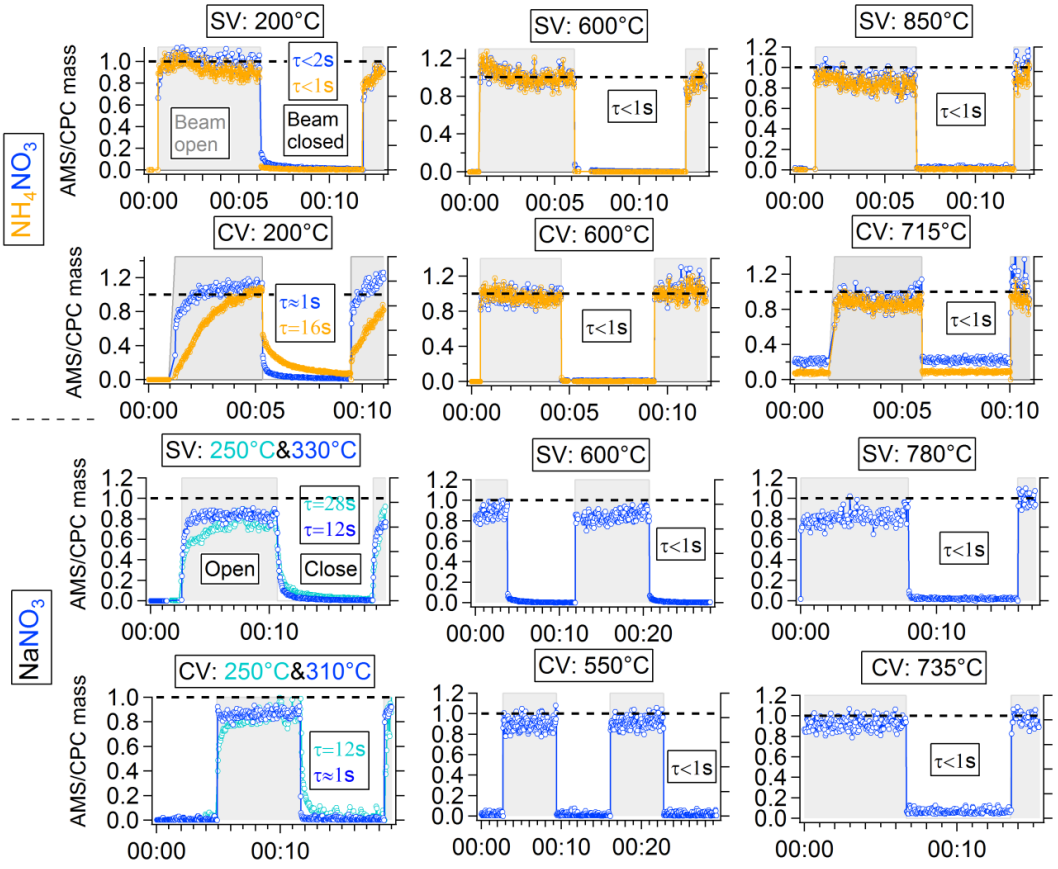

FIG. 10 Results of an experiment slowly alternating beam-open and beam-closed positions while sampling NH_4NO_3 and $NaNO_3$ in the SV and CV. Note that the total signal (and not just the difference signal) is shown in all panels. The results from three/four different vaporizer temperatures (low, medium and high within the usable range) for each species are shown. τ is the lifetime of signal decay and was estimated through an exponential fit to the relevant part of the time series. τ for the rising signal is not shown, since it always varies in the same way.

Atmos. Meas. Tech. Discuss., doi:10.5194/amt-2016-337, 2016
Manuscript under review for journal Atmos. Meas. Tech.
Published: 9 November 2016

Atmospheric Measurement Techniques Discussions

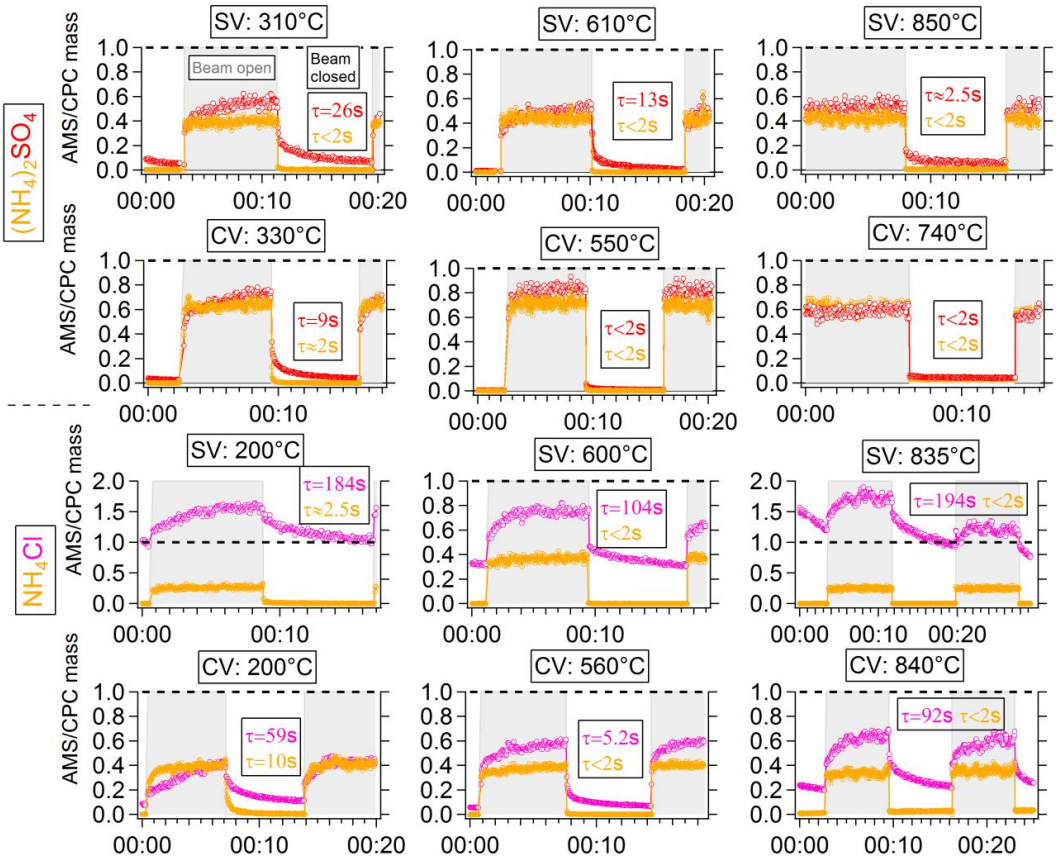

FIG. 11 Results of an experiment slowly alternating beam-open and beam-closed positions while sampling $NaNO_3$ and NH_4Cl in the SV and CV. Note that the total signal (and not just the difference signal) is shown in all panels. The results from three/four different vaporizer temperatures (low, medium and high within the usable range) for each species are shown. T is the lifetime of signal decay and was estimated through an exponential fit to the relevant part of the time series. τ for the rising signal is not shown, since it varies in the same way.

Atmos. Meas. Tech. Discuss., doi:10.5194/amt-2016-337, 2016
Manuscript under review for journal Atmos. Meas. Tech.
Published: 9 November 2016

Atmospheric Measurement Techniques Discussions

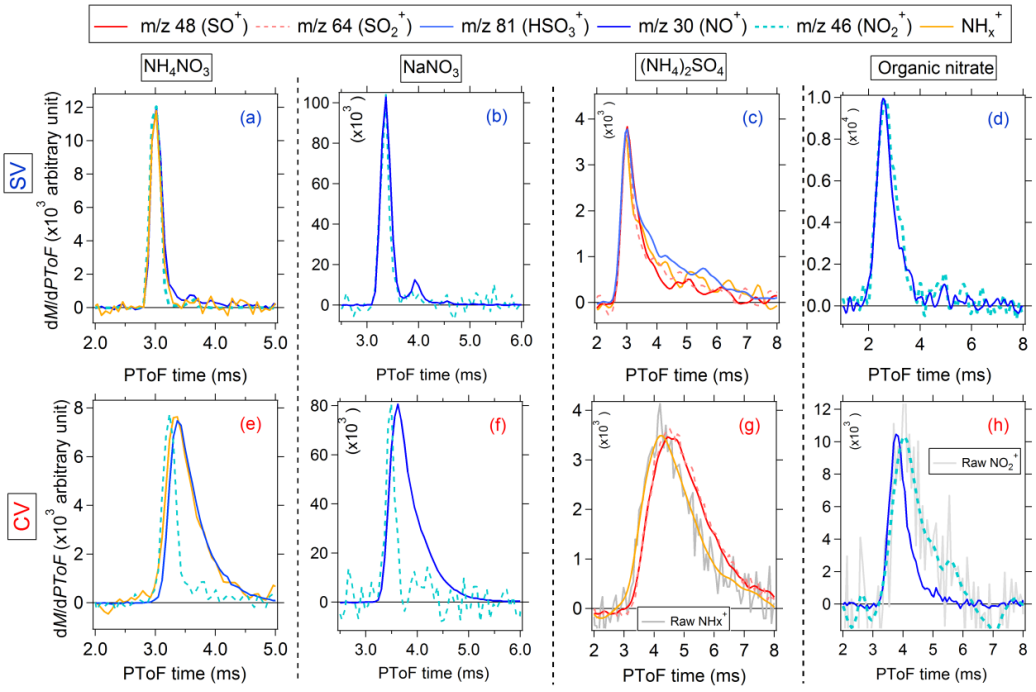

FIG. 12 Size-resolved detection (using the PToF acquisition mode) for major ions from 300 nm NH_4NO_3, 300 nm $NaNO_3$, 250 nm $(NH_4)_2SO_4$ and chamber-produced organic nitrate in the SV and CV at T_v ~ 500-650℃. The PToF distributions of NH_x^+ in Fig. 12(g) and of NO_2^+ in Fig. 12(h) were smoothed.

Atmos. Meas. Tech. Discuss., doi:10.5194/amt-2016-337, 2016
Manuscript under review for journal Atmos. Meas. Tech.
Published: 9 November 2016

Atmospheric Measurement Techniques
Discussions

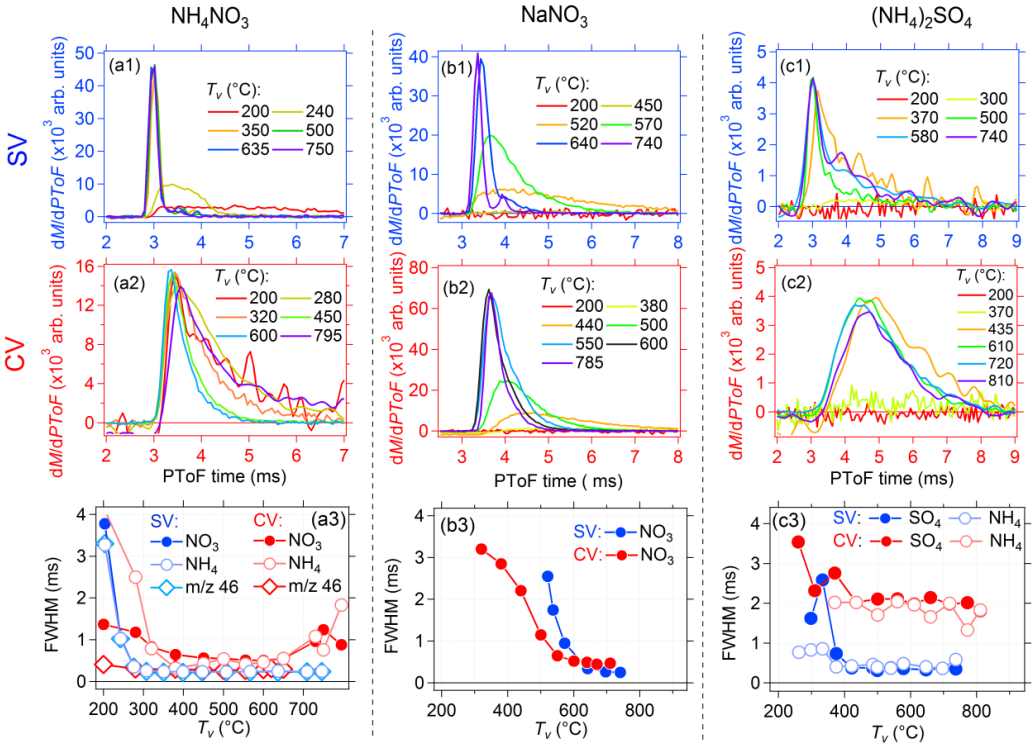

FIG. 13 Size-resolved detection of (a) 250 nm $(NH_4)_2SO_4$, (b) 300 nm NH_4NO_3 and (c) 300 nm $NaNO_3$ using the PToF acquisition mode from the SV and CV as a function of T_v. Particle peak widths of (a3) NH_4NO_3, (b3) $NaNO_3$ and (c3) $(NH_4)_2SO_4$ as a function of T_v are also shown.

Atmos. Meas. Tech. Discuss., doi:10.5194/amt-2016-337, 2016
Manuscript under review for journal Atmos. Meas. Tech.
Published: 9 November 2016

Atmospheric Measurement Techniques Discussions

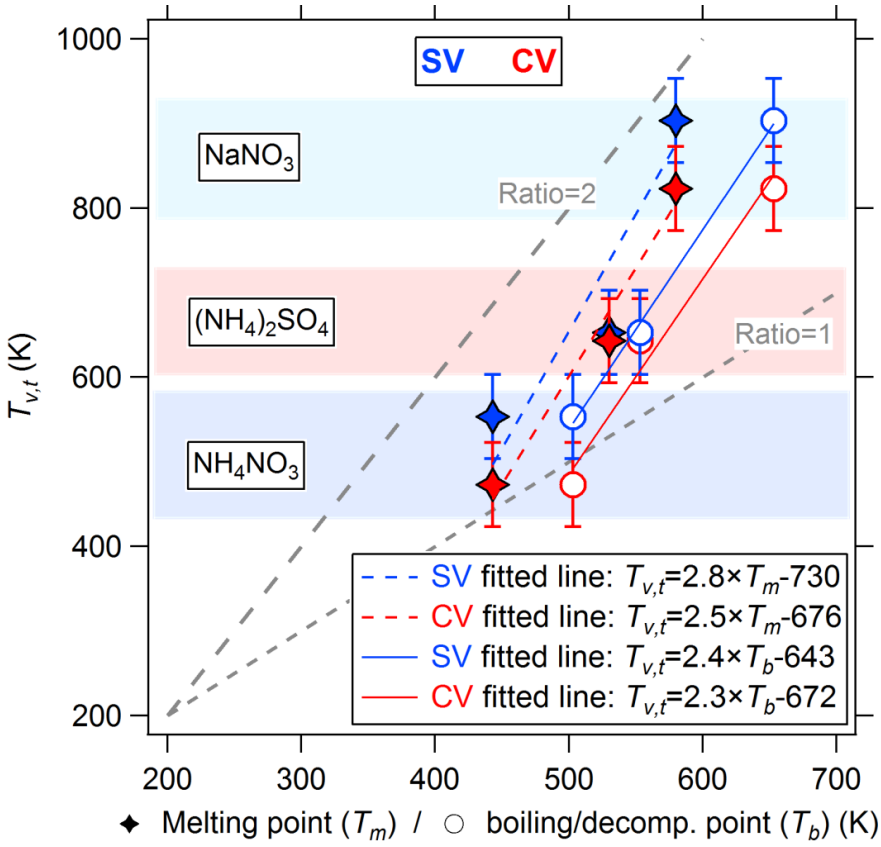

FIG. 14 scatter plot between transition T_v ($T_{v,t}$) and melting points (T_m) and boiling/decomposition points (T_b) of three standard species in both SV and CV. The boiling point of $(NH_4)_2SO_4$ is its decomposition temperature (Haynes, 2015).

Atmos. Meas. Tech. Discuss., doi:10.5194/amt-2016-337, 2016
Manuscript under review for journal Atmos. Meas. Tech.
Published: 9 November 2016

Atmospheric Measurement Techniques
Discussions

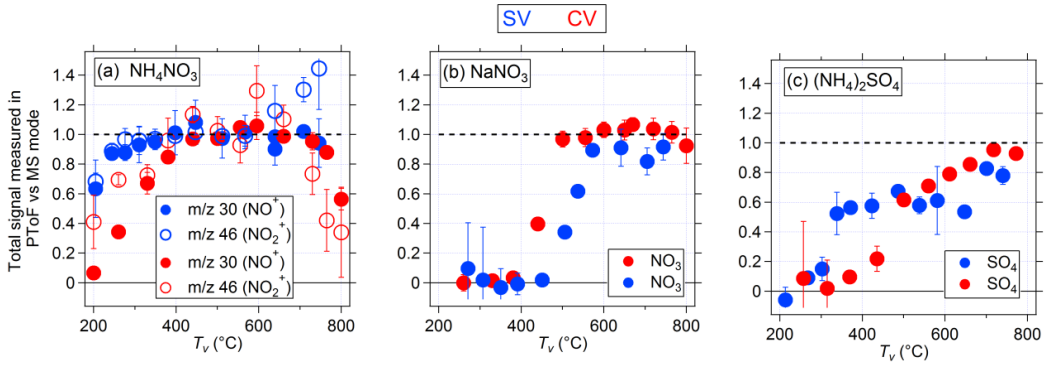

FIG. 15 Ratio of total signals measured in PToF vs MS mode for (a) $(NH_4)_2SO_4$, (b) NH_4NO_3 and (c) $NaNO_3$ in the SV and CV as a function of T_v.

References

Allan, J. D., Alfarra, M. R., Bower, K. N., Williams, P. I., Gallagher, M. W., Jimenez, J. L., McDonald, A. G., Nemitz, E., Canagaratna, M. R., Jayne, J. T., Coe, H., and Worsnop, D. R.: Quantitative sampling using an Aerodyne aerosol mass spectrometer - 2. Measurements of fine particulate chemical composition in two U.K. cities, J Geophys. Res.-Atmos, 108, D3, 4091, Doi 10.1029/2002jd002359, 2003a.

Allan, J. D., Jimenez, J. L., Williams, P. I., Alfarra, M. R., Bower, K. N., Jayne, J. T., Coe, H., and Worsnop, D. R.: Quantitative sampling using an Aerodyne aerosol mass spectrometer: 1. Techniques of data interpretation and error analysis J Geophys. Res.-Atmos, 108, Doi 10.1029/2003jd001607, 2003b.

Allan, J. D., Bower, K. N., Coe, H., Boudries, H., Jayne, J. T., Canagaratna, M. R., Millet, D. B., Goldstein, A. H., Quinn, P. K., Weber, R. J., and Worsnop, D. R.: Submicron aerosol composition at Trinidad Head, California, during ITCT 2K2: Its relationship with gas phase volatile organic carbon and assessment of instrument performance, J Geophys. Res.-Atmos, 109, Doi 10.1029/2003jd004208, 2004a.

Allan, J. D., Delia, A. E., Coe, H., Bower, K. N., Alfarra, M. R., Jimenez, J. L., Middlebrook, A. M., Drewnick, F., Onasch, T. B., Canagaratna, M. R., Jayne, J. T., and Worsnop, D. R.: A generalised method for the extraction of chemically resolved mass spectra from aerodyne aerosol mass spectrometer data, J Aerosol Sci., 35, 909-922, DOI 10.1016/j.jaerosci.2004.02.007, 2004b.

Bae, M. S., Schwab, J. J., Zhang, Q., Hogrefe, O., Demerjian, K. L., Weimer, S., Rhoads, K., Orsini, D., Venkatachari, P., and Hopke, P. K.: Interference of organic signals in highly time resolved nitrate measurements by low mass resolution aerosol mass spectrometry, J Geophys. Res.-Atmos, 112, Doi 10.1029/2007jd008614, 2007.

Bahreini, R., Keywood, M. D., Ng, N. L., Varutbangkul, V., Gao, S., Flagan, R. C., Seinfeld, J. H., Worsnop, D. R., and Jimenez, J. L.: Measurements of Secondary Organic Aerosol from Oxidation of Cycloalkenes, Terpenes, and m-Xylene Using an Aerodyne Aerosol Mass Spectrometer, Environ Sci. Technol., 39, 5674-5688, 10.1021/es048061a, 2005.

Bahreini, R., Dunlea, E. J., Matthew, B. M., Simons, C., Docherty, K. S., DeCarlo, P. F., Jimenez, J. L., Brock, C. A., and Middlebrook, A. M.: Design and operation of a pressure-controlled inlet for airborne sampling with an aerodynamic aerosol lens, Aerosol Sci Tech, 42, 465-471, Doi 10.1080/02786820802178514, 2008.

Bahreini, R., Ervens, B., Middlebrook, A. M., Warneke, C., de Gouw, J. A., DeCarlo, P. F., Jimenez, J. L., Brock, C. A., Neuman, J. A., Ryerson, T. B., Stark, H., Atlas, E., Brioude, J., Fried, A., Holloway, J. S., Peischl, J., Richter, D., Walega, J., Weibring, P., Wollny, A. G., and Fehsenfeld, F. C.: Organic aerosol formation in urban and industrial plumes near Houston and Dallas, Texas, J Geophys. Res.-Atmos, 114, D00F16, 10.1029/2008jd011493, 2009.

Bruns, E. A., Perraud, V., Zelenyuk, A., Ezell, M. J., Johnson, S. N., Yu, Y., Imre, D., Finlayson-Pitts, B. J., and Alexander, M. L.: Comparison of FTIR and Particle Mass Spectrometry for the Measurement of Particulate Organic Nitrates, Environ. Sci. Technol., 44, 1056-1061, 10.1021/es9029864, 2010.

Canagaratna, M. R., Jayne, J. T., Jimenez, J. L., Allan, J. D., Alfarra, M. R., Zhang, Q., Onasch, T. B., Drewnick, F., Coe, H., Middlebrook, A., Delia, A., Williams, L. R., Trimborn, A. M., Northway, M. J., DeCarlo, P. F., Kolb, C. E., Davidovits, P., and Worsnop, D. R.: Chemical and microphysical characterization of ambient aerosols with the aerodyne aerosol mass spectrometer, Mass Spectrom Rev., 26, 185-222, Doi 10.1002/Mas.20115, 2007.

Canagaratna, M. R., Jimenez, J. L., Kroll, J. H., Chen, Q., Kessler, S. H., Massoli, P., Hildebrandt Ruiz, L., Fortner, E., Williams, L. R., Wilson, K. R., Surratt, J. D., Donahue, N. M., Jayne, J. T., and Worsnop, D. R.: Elemental ratio measurements of organic compounds using aerosol mass spectrometry: characterization, improved calibration, and implications, Atmos. Chem. Phys., 15, 253-272, 10.5194/acp-15-253-2015, 2015.

DeCarlo, P. F., Slowik, J. G., Worsnop, D. R., Davidovits, P., and Jimenez, J. L.: Particle morphology and density characterization by combined mobility and aerodynamic diameter measurements. Part 1: Theory, Aerosol Sci. Tech., 38, 1185-1205, Doi 10.1080/027868290903907, 2004.

DeCarlo, P. F., Kimmel, J. R., Trimborn, A., Northway, M. J., Jayne, J. T., Aiken, A. C., Gonin, M., Fuhrer, K., Horvath, T., Docherty, K. S., Worsnop, D. R., and Jimenez, J. L.: Field-deployable, high-resolution, time-of-flight aerosol mass spectrometer, Anal. Chem., 78, 8281-8289, Doi 10.1021/Ac061249n, 2006.

Docherty, K. S., Aiken, A. C., Huffman, J. A., Ulbrich, I. M., DeCarlo, P. F., Sueper, D., Worsnop, D. R., Snyder, D. C., Peltier, R. E., Weber, R. J., Grover, B. D., Eatough, D. J., Williams, B. J., Goldstein, A. H., Ziemann, P. J., and Jimenez, J. L.: The 2005 Study of Organic Aerosols at Riverside (SOAR-1): instrumental intercomparisons and fine particle composition, Atmos. Chem. Phys., 11, 12387-12420, 10.5194/acp-11-12387-2011, 2011.

Docherty, K. S., Jaoui, M., Corse, E., Jimenez, J. L., Offenberg, J. H., Lewandowski, M., and Kleindienst, T. E.: Collection Efficiency of the Aerosol Mass Spectrometer for Chamber-Generated Secondary Organic Aerosols, Aerosol Sci. Tech., 47, 294-309, 10.1080/02786826.2012.752572, 2012.

Docherty, K. S., Lewandowski, M., and Jimenez, J. L.: Effect of Vaporizer Temperature on Ambient Non-Refractory Submicron Aerosol Composition and Mass Spectra Measured by the Aerosol Mass Spectrometer, Aerosol Sci. Tech., 49, 485-494, 10.1080/02786826.2015.1042100, 2015.

Drewnick, F., Schwab, J. J., Hogrefe, O., Peters, S., Husain, L., Diamond, D., Weber, R., and Demerjian, K. L.: Intercomparison and evaluation of four semi-continuous PM2.5 sulfate instruments, Atmos. Environ., 37, 3335-3350, Doi 10.1016/S1352-2310(03)00351-0, 2003.

Drewnick, F., Jayne, J. T., Canagaratna, M., Worsnop, D. R., and Demerjian, K. L.: Measurement of ambient aerosol composition during the PMTACS-NY 2001 using an aerosol mass spectrometer. Part II: Chemically speciated mass distributions, Aerosol Sci. Tech., 38, 104-117, Doi 10.1080/02786820390229534, 2004a.

Drewnick, F., Schwab, J. J., Jayne, J. T., Canagaratna, M., Worsnop, D. R., and Demerjian, K. L.: Measurement of ambient aerosol composition during the PMTACS-NY 2001 using an aerosol mass spectrometer. Part I: Mass concentrations, Aerosol Sci. Tech., 38, 92-103, Doi 10.1080/02786820390229507, 2004b.

Drewnick, F., Diesch, J. M., Faber, P., and Borrmann, S.: Aerosol mass spectrometry: particle–vaporizer interactions and their consequences for the measurements, Atmos. Meas. Tech., 8, 3811-3830, 10.5194/amt-8-3811-2015, 2015.

Farmer, D. K., and Jimenez, J. L.: Real-time Atmospheric Chemistry Field Instrumentation, Anal. Chem., 82, 7879-7884, Doi 10.1021/Ac1010603, 2010.

Friedel, R. A., Shultz, J. L., and Sharkey, A. G.: Mass Spectrum of Nitric Acid, Anal. Chem., 31, 1128-1128, 10.1021/ac60150a615, 1959.

Fry, J. L., Draper, D. C., Zarzana, K. J., Campuzano-Jost, P., Day, D. A., Jimenez, J. L., Brown, S. S., Cohen, R. C., Kaser, L., Hansel, A., Cappellin, L., Karl, T., Hodzic Roux, A., Turnipseed, A., Cantrell, C., Lefer, B. L., and Grossberg, N.: Observations of gas- and aerosol-phase organic nitrates at BEACHON-RoMBAS 2011, Atmos. Chem. Phys., 13, 8585-8605, 10.5194/acp-13-8585-2013, 2013.

Fuzzi, S., Baltensperger, U., Carslaw, K., Decesari, S., Denier van der Gon, H., Facchini, M. C., Fowler, D., Koren, I., Langford, B., Lohmann, U., Nemitz, E., Pandis, S., Riipinen, I., Rudich, Y., Schaap, M., Slowik, J. G., Spracklen, D. V., Vignati, E., Wild, M., Williams, M., and Gilardoni, S.: Particulate matter, air quality and climate: lessons learned and future needs, Atmos. Chem. Phys., 15, 8217-8299, 10.5194/acp-15-8217-2015, 2015.

Hallquist, M., Wenger, J. C., Baltensperger, U., Rudich, Y., Simpson, D., Claeys, M., Dommen, J., Donahue, N. M., George, C., Goldstein, A. H., Hamilton, J. F., Herrmann, H., Hoffmann, T., Iinuma, Y., Jang, M., Jenkin, M. E., Jimenez, J. L., Kiendler-Scharr, A., Maenhaut, W., McFiggans, G., Mentel, T. F., Monod, A., Prevot, A. S. H., Seinfeld, J. H., Surratt, J. D.,

Szmigielski, R., and Wildt, J.: The formation, properties and impact of secondary organic aerosol: current and emerging issues, Atmos. Chem. Phys., 9, 5155-5236, 2009.

Haynes, W.: CRC Handbook of Chemistry and Physics (96th ed.), CRC Press, 2015.

Heal, M. R., Kumar, P., and Harrison, R. M.: Particles, air quality, policy and health, Chem. Soc. Rev., 41, 6606-6630, 2012.

Hogrefe, O., Drewnick, F., Lala, G. G., Schwab, J. J., and Demerjian, K. L.: Development, operation and applications of an aerosol generation, calibration and research facility, Aerosol Sci Tech, 38, 196-214, Doi 10.1080/02786820390229516, 2004.

Hu, W., Hu, M., Hu, W., Jimenez, J. L., Yuan, B., Chen, W., Wang, M., Wu, Y., Chen, C., Wang, Z., Peng, J., Zeng, L., and Shao, M.: Chemical composition, sources and aging process of sub-micron aerosols in Beijing: contrast between summer and winter, J Geophys. Res.-Atmos, 121, 1955-1977, 10.1002/2015jd024020, 2016.

Huffman, J. A., Jayne, J. T., Drewnick, F., Aiken, A. C., Onasch, T., Worsnop, D. R., and Jimenez, J. L.: Design, modeling, optimization, and experimental tests of a particle beam width probe for the aerodyne aerosol mass spectrometer, Aerosol Sci. Tech., 39, 1143-1163, Doi 10.1080/02786820500423782, 2005.

Huffman, J. A., Ziemann, P. J., Jayne, J. T., Worsnop, D. R., and Jimenez, J. L.: Development and Characterization of a Fast-Stepping/Scanning Thermodenuder for Chemically-Resolved Aerosol Volatility Measurements (vol 42, pg 395, 2008), Aerosol Sci. Tech., 43, 273-273, Doi 10.1080/02786820802616885, 2009.

IPCC: Climate Change 2013: The Physical Science Basis. Contribution of Working Group I to the Fifth Assessment Report of the Intergovernmental Panel on Climate Change, Cambridge University Press, Cambridge, United Kingdom and New York, NY, USA, 1535 pp., 2013.

Jayne, J. T., Leard, D. C., Zhang, X. F., Davidovits, P., Smith, K. A., Kolb, C. E., and Worsnop, D. R.: Development of an aerosol mass spectrometer for size and composition analysis of submicron particles, Aerosol Sci. Tech., 33, 49-70, 2000.

Jayne, J. T., and Worsnop, D. R.: Particle capture device, Aerodyne Research, Inc. , 20150040689 A1, 2016.

Jimenez, J. L., Jayne, J. T., Shi, Q., Kolb, C. E., Worsnop, D. R., Yourshaw, I., Seinfeld, J. H., Flagan, R. C., Zhang, X. F., Smith, K. A., Morris, J. W., and Davidovits, P.: Ambient aerosol sampling using the Aerodyne Aerosol Mass Spectrometer, J Geophys. Res.-Atmos, 108, 8425, Doi 10.1029/2001jd001213, 2003.

Jimenez, J. L., Canagaratna, M. R., Donahue, N. M., Prevot, A. S. H., Zhang, Q., Kroll, J. H., DeCarlo, P. F., Allan, J. D., Coe, H., Ng, N. L., Aiken, A. C., Docherty, K. S., Ulbrich, I. M., Grieshop, A. P., Robinson, A. L., Duplissy, J., Smith, J. D., Wilson, K. R., Lanz, V. A., Hueglin, C., Sun, Y. L., Tian, J., Laaksonen, A., Raatikainen, T., Rautiainen, J., Vaattovaara, P., Ehn, M., Kulmala, M., Tomlinson, J. M., Collins, D. R., Cubison, M. J., Dunlea, E. J., Huffman, J. A., Onasch, T. B., Alfarra, M. R., Williams, P. I., Bower, K., Kondo, Y., Schneider, J., Drewnick, F., Borrmann, S., Weimer, S., Demerjian, K., Salcedo, D., Cottrell, L., Griffin, R., Takami, A., Miyoshi, T., Hatakeyama, S., Shimono, A., Sun, J. Y., Zhang, Y. M., Dzepina, K., Kimmel, J. R., Sueper, D., Jayne, J. T., Herndon, S. C., Trimborn, A. M., Williams, L. R., Wood, E. C., Middlebrook, A. M., Kolb, C. E., Baltensperger, U., and Worsnop, D. R.: Evolution of Organic Aerosols in the Atmosphere, Science, 326, 1525-1529, DOI 10.1126/science.1180353, 2009.

Jimenez, J. L., Canagaratna, M. R., Drewnick, F., Allan, J. D., Alfarra, M. R., Middlebrook, A. M., Slowik, J. G., Zhang, Q., Coe, H., Jayne, J. T., and Worsnop, D. R.: Comment on "The effects of molecular weight and thermal decomposition on the sensitivity of a thermal desorption aerosol mass spectrometer", Aerosol Sci. Tech., 50, i-xv, 10.1080/02786826.2016.1205728, 2016.

Kang, M., Cho, H.-J., Kwak, H., and Park, K.: Evaluation of Particle Bounce in Various Collection Substrates to be Used as Vaporizer in Aerosol Mass Spectrometer, Aerosol Sci. Tech., 49, 332-339, 10.1080/02786826.2015.1028518, 2015.

Knote, C., Brunner, D., Vogel, H., Allan, J., Asmi, A., Äijälä, M., Carbone, S., van der Gon, H. D., Jimenez, J. L., Kiendler-Scharr, A., Mohr, C., Poulain, L., Prévôt, A. S. H., Swietlicki, E., and Vogel, B.: Towards an online-coupled chemistry-climate model: evaluation of trace gases and aerosols in COSMO-ART, Geosci. Model Dev., 4, 1077-1102, 10.5194/gmd-4-1077-2011, 2011.

Linstrom, P. J., and Mallard, W. G.: NIST Chemistry WebBook, NIST Standard Reference Database Number 69, 2016.

Liu, P., Ziemann, P. J., Kittelson, D. B., and Mcmurry, P. H.: Generating Particle Beams of Controlled Dimensions and Divergence .1. Theory of Particle Motion in Aerodynamic Lenses and Nozzle Expansions, Aerosol Sci. Tech., 22, 293-313, 1995a.

Liu, P., Ziemann, P. J., Kittelson, D. B., and McMurry, P. H.: Generating Particle Beams of Controlled Dimensions and Divergence: II. Experimental Evaluation of Particle Motion in Aerodynamic Lenses and Nozzle Expansions, Aerosol Sci. Tech., 22, 314-324, 10.1080/02786829408959749, 1995b.

Liu, P. S. K., Deng, R., Smith, K. A., Williams, L. R., Jayne, J. T., Canagaratna, M. R., Moore, K., Onasch, T. B., Worsnop, D. R., and Deshler, T.: Transmission efficiency of an aerodynamic focusing lens system: Comparison of model calculations and laboratory measurements for the Aerodyne Aerosol Mass Spectrometer, Aerosol Sci. Tech., 41, 721-733, Doi 10.1080/02786820701422278, 2007.

Matthew, B. M., Middlebrook, A. M., and Onasch, T. B.: Collection efficiencies in an Aerodyne Aerosol Mass Spectrometer as a function of particle phase for laboratory generated aerosols, Aerosol Sci. Tech., 42, 884-898, Doi 10.1080/02786820802356797, 2008.

Middlebrook, A. M., Bahreini, R., Jimenez, J. L., and Canagaratna, M. R.: Evaluation of Composition-Dependent Collection Efficiencies for the Aerodyne Aerosol Mass Spectrometer using Field Data, Aerosol Sci. Tech., 46, 258-271, 10.1080/02786826.2011.620041, 2012.

Murphy, D. M.: The effects of molecular weight and thermal decomposition on the sensitivity of a thermal desorption aerosol mass spectrometer, Aerosol Sci. Tech., 50, 118-125, 10.1080/02786826.2015.1136403, 2016.

Ozawa, Y., Takeda, N., Miyakawa, T., Takei, M., Hirayama, N., and Takegawa, N.: Evaluation of a particle trap laser desorption mass spectrometer (PT-LDMS) for the quantification of sulfate aerosols, Aerosol Sci. Tech., 00-00, 10.1080/02786826.2016.1139685, 2016.

Pieber, S. M., El Haddad, I., Slowik, J. G., Canagaratna, M. R., Jayne, J. T., Platt, S. M., Bozzetti, C., Daellenbach, K. R., Fröhlich, R., Vlachou, A., Klein, F., Dommen, J., Miljevic, B., Jiménez, J. L., Worsnop, D. R., Baltensperger, U., and Prévôt, A. S. H.: Inorganic Salt Interference on CO2+ in Aerodyne AMS and ACSM Organic Aerosol Composition Studies, Environ Sci. Technol., 10.1021/acs.est.6b01035, 2016.

Quinn, P. K., Bates, T. S., Coffman, D., Onasch, T. B., Worsnop, D., Baynard, T., de Gouw, J. A., Goldan, P. D., Kuster, W. C., Williams, E., Roberts, J. M., Lerner, B., Stohl, A., Pettersson, A., and Lovejoy, E. R.: Impacts of sources and aging on submicrometer aerosol properties in the marine boundary layer across the Gulf of Maine, J Geophys. Res.-Atmos, 111, 10.1029/2006JD007582, 2006.

Salcedo, D., Onasch, T. B., Canagaratna, M. R., Dzepina, K., Huffman, J. A., Jayne, J. T., Worsnop, D. R., Kolb, C. E., Weimer, S., Drewnick, F., Allan, J. D., Delia, A. E., and Jimenez, J. L.: Technical Note: Use of a beam width probe in an Aerosol Mass Spectrometer to monitor particle collection efficiency in the field, Atmos. Chem. Phys., 7, 549-556, 2007.

Takegawa, N., Miyakawa, T., Watanabe, M., Kondo, Y., Miyazaki, Y., Han, S., Zhao, Y., van Pinxteren, D., Bruggemann, E., Gnauk, T., Herrmann, H., Xiao, R., Deng, Z., Hu, M., Zhu, T., and Zhang, Y.: Performance of an Aerodyne Aerosol Mass Spectrometer (AMS) during Intensive Campaigns in China in the Summer of 2006, Aerosol Sci. Tech., 43, 189-204, Doi 10.1080/02786820802582251, 2009.

Takegawa, N., Miyakawa, T., Nakamura, T., Sameshima, Y., Takei, M., Kondo, Y., and Hirayama, N.: Evaluation of a New Particle Trap in a Laser Desorption Mass Spectrometer for Online

Measurement of Aerosol Composition, Aerosol Sci. Tech., 46, 428-443, 10.1080/02786826.2011.635727, 2012.

Turpin, B. J., Saxena, P., and Andrews, E.: Measuring and simulating particulate organics in the atmosphere: problems and prospects, Atmos Environ, 34, 2983-3013, 2000.

Wang, Z., Lu, P., Zhang, X., Wang, L., Li, Q., and Zhang, Z.: NOx storage and soot combustion over well-dispersed mesoporous mixed oxides via hydrotalcite-like precursors, RSC Advances, 5, 52743-52753, 10.1039/c5ra07414b, 2015.

Weimer, S., Drewnick, F., Hogrefe, O., Schwab, J. J., Rhoads, K., Orsini, D., Canagaratna, M., Worsnop, D. R., and Demerjian, K. L.: Size-selective nonrefractory ambient aerosol measurements during the Particulate Matter Technology Assessment and Characterization Study - New York 2004 Winter Intensive in New York City, J Geophys. Res.-Atmos, 111, Doi 10.1029/2006jd007215, 2006.

Williams, L.: What is My Vaporizer Temperature?, AMS user's meeting, Hyytiala, Finland, 2010.

Xu, W., Croteau, P., Williams, L., Canagaratna, M., Onasch, T., Cross, E., Zhang, X., Robinson, W., Worsnop, D., and Jayne, J.: Laboratory characterization of an aerosol chemical speciation monitor with PM2.5 measurement capability, Aerosol Sci. Tech., 1-15, 10.1080/02786826.2016.1241859, 2016.

Zhu, R. S., Wang, J. H., and Lin, M. C.: Sublimation of Ammonium Salts: A Mechanism Revealed by a First-Principles Study of the NH4Cl System, The Journal of Physical Chemistry C, 111, 13831-13838, 10.1021/jp073448w, 2007.